ULTRASONIC SURFACE WAVE TRANSDUCERS

Otto Gal

A TECHNICAL REPORT

in

Faculty

of

Engineering

Presented in partial fulfilment of the requirements for
the Degree of Master of Engineering at
Sir George Williams University
Montreal, Canada

September, 1972

TABLE OF CONTENTS

LIST OF TABLES

LIST OF FIGURES

ACKNOWLEDGEMENTS

I wish to extend my thanks to Prof. O. Schwelb for his guidance and helpful suggestions during the progress of this work.

Thanks are also due to my wife, Susan, for her most valuable help in typing this report.

ABSTRACT

Ultrasonic Surface Wave Transducers

Conditions for the propagation of surface elastic waves are discussed under a variety of conditions. Emphasis is placed on piezoelectric materials. A description of the many ways of transduction is followed by a detailed examination of interdigital electrode arrays on piezoelectric crystal substrates.

Design considerations of simple uniform arrays and transducers of variable spacing are treated, together with typical applications of surface wave devices. Properties of the more frequently used substrate materials are evaluated. Methods of device fabrication and measurement of their characteristics are examined, along with special considerations of microwave frequency operation.

CHAPTER 1

INTRODUCTION

A new family of electronic devices is growing up, based on surface acoustic wave propagation. The waves involved are elastic stress-waves, propagating along the surface of a crystal. Their main distinguishing feature is their low velocity, about 5 orders of magnitude slower than electromagnetic waves.

Seismologists have been aware of elastic wave propagation since the last century and significant research by Lord Rayleigh and others has been accomplished in the early years. The current interest is due not only to the many attractive characteristics of such waves, but also the rapid advances in the techniques for the manufactrue of integrated circuits. These techniques can be directly applied to the fabrication of surface acoustic devices. Hence, they can be expected to be reliable, reproducible and inexpensive.

Other attractive features include compactness: because of the slow propagational velocity, delay lines, filters, etc. can be constructed with dimensions which are small physically, yet sizeable electrically in terms of wavelength. They also offer multifunction capability, as the wave is accessible for sampling along its entire path of propagation.

Surface acoustic wave propagation can take several

different forms, such as Rayleigh waves, Love waves and Stoneley waves. Rayleigh waves, the most frequently used in present-day devices, are waves which propagate along the free surface of solid substrates and involve elliptically polarized particle displacements that decay exponentially with depth [26].

These waves, which are dispersionless, propagate at a typical velocity of 3×10^5 cm/sec and exhibit low attenuation in certain crystalline media such as $LiNbO_3$ or single crystal quartz, typically about 0.1 db/cm or 1.5×10^{-4} db/wavelength. The slow velocity gives delays of about 3 μsec/cm and wavelengths of about 30 μm at 100 MHz.

In most practical cases the acoustic medium is a piezoelectric crystal, permitting the launching and detection of the waves by electrodes on the surface. In this case, the external stimulus is in the form of an electric signal, which gives rise to stresses on the piezoelectric surface.

The operation of the various types of such electrodes, usually, thin metallic strips deposited on the crystal surface, is the main subject of this report.

CHAPTER 2

ACOUSTIC PROPAGATION

2.1 Bulk waves

Electroacoustic devices operate through the utilization of elastic waves propagating in crystal medium. Early models employed bulk elastic waves, i.e. wave propagating in the interior (or bulk) of the crystal. Although surface wave devices have displaced bulk wave devices in most applications, the latter are still competitive in certain fields, such as delay lines of fixed delay. The appeal of bulk waves lies mostly in their lower attenuation and their ability to function at microwave frequencies. Since the bulk waves are less complicated to describe mathematically than their surface wave counterparts, they serve well to introduce many of the concepts to be used later in analyzing surface waves. The following analytical treatment is largely based on the work of G.W. Farnell [16].

One of the simplest media to treat is one which is perfectly elastic, homogeneous but anisotropic [50]. The stress, T (force per unit area) and the strain, S (normalized particle displacement) are related by Hooke's Law:

$$T_{ij} = C_{ijkl}\, S_{kl} \tag{1}$$

$$\text{where } S_{kl} = \frac{1}{2}\left(\frac{\partial u_k}{\partial x_l} + \frac{\partial u_l}{\partial x_k}\right) \tag{2}$$

where u_k is the displacement component in the k direction,

x_l is the l^{th} position coordinate, T_{ij} is the stress along the i coordinate direction on a surface the normal of which is parallel to the x_j axes in a Cartesian coordinate system, C_{ijkl} is the stiffness tensor. Combined with Newton's force equation, the above relations can be combined into the elastic wave equation:

$$\rho \frac{\partial^2 u_j}{\partial t^2} = C_{ijkl} \frac{\partial^2 u_k}{\partial x_i \partial x_l} \qquad (i,j,k,l = 1,2,3) \qquad (3)$$

where summation for repeated indices is assumed (ρ is the density of the medium).

In an infinite medium, the solution of the wave equation has the form

$$\bar{u} = \bar{A} \exp\left[ik \quad (l_i x_i - vt)\right] \qquad (4)$$

with $\bar{A} = \bar{i}_j \alpha_j$ where $\bar{i}_j$ is a unit vector along the x_j axis and v is the phase velocity of the wave in the direction of the propagation vector $\bar{k}$ whose directional cosines are l_i.

The solution describes plane waves. By substituting the above form of solution into the wave equation, a cubic equation in v^2 results whose three roots lead to three mutually perpendicular displacement vectors: one quasi—longitudinal the other two quasi—transverse. In case of propagation along high-symmetry directions in a crystal, the displacements become purely longitudinal and transverse respectively. The nature of particle movement within the crystal in such a case is displayed

by Fig. 1. The two sketches show the instantaneous positions of particles (along a section of the crystal made in the direction of propagation) due to longitudinal component only (Fig. 1(a)), or a transverse component only (Fig. 1(b)). The three directions of displacement involve different velocities. Transverse waves are slower than longitudinal ones by a factor which depends on the particular bulk material, but generally is in the order of 1.5 to 2.5. Significantly, the phase velocities of bulk waves are frequency-independent over the spectrum of practical interest, and are numerically equal to the square root of a linear combination of elastic stiffness constants divided by the mass density of the solid.

Next, the effect of piezoelectricity may be considered. The presence of such a property in the crystal will alter somewhat the velocities previously determined. The wave equations can now be rewritten as follows:

$$\rho \frac{\partial^2 u_j}{\partial t^2} - c_{ijkl} \frac{\partial^2 u_k}{\partial x_i \partial x_l} - e_{kij} \frac{\partial^2 \phi}{\partial x_k \partial x_i} = 0 \qquad (5)$$

$$e_{ikl} \frac{\partial^2 u_k}{\partial x_i \partial x_l} - \varepsilon_{ik} \frac{\partial^2 \phi}{\partial x_k \partial x_i} = 0 \qquad (6)$$

$i,j,k,l = 1,2,3$

The new symbols represent the following:

e_{kij} is the piezoelectric tensor

ε_{ik} is the dielectric permittivity tensor

ϕ is the scalar potential

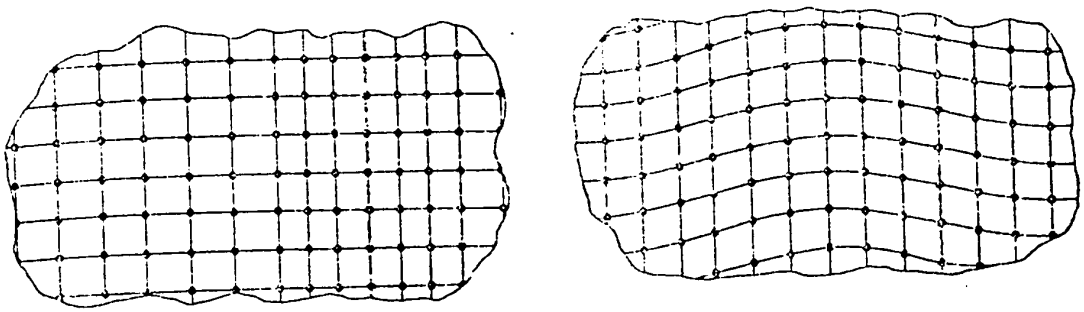

(a) (b)

Fig. 1 Longitudinal and transverse waves

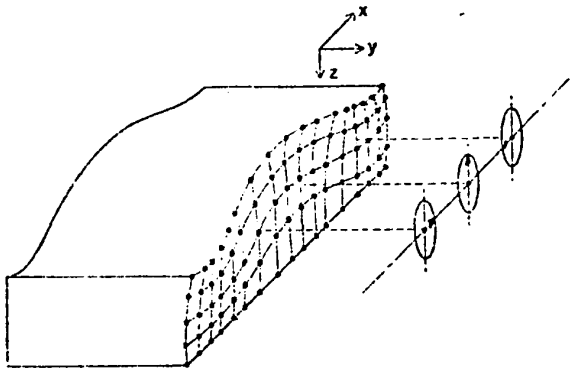

Fig. 2 Rayleigh waves

The electric field is simply the negative gradient of ϕ, since the low velocity of acousto-electric waves causes the magnetic field to be negligibly small. The overall effect of piezoelectricity on the solution of the wave equation is the appearance of a modified stiffness tensor.

$$C'_{ijkl} = C_{ijkl} + (e_{mij}\, e_{nkl}\, l_m l_n / \varepsilon_{pq}\, l_p\, l_q) \qquad (7)$$

In any one direction $c' = c\,(1+k^2)$ where k is the electromechanical coupling coefficient, a measure of the strength of piezoelectricity in the crystal. Obviously, the piezoelectric coupling increased the value of c, or it "stiffened" the material, with the consequent increase in wave velocity. For materials with weak coupling (small k), the effect is too small to be of importance, but for a few crystals, such as lithium niobate for example, it is significant. Neglecting it would result in an error of about 15% in calculating wave velocity.

Materials with strong piezoelectric properties are widely used for acoustic device substrates, for bulk as well as surface wave devices. The reason for this is the relative ease with which electric signals can be converted into elastic waves by means of metallic electrodes placed on the crystal. Yet, the use of these materials sometimes has disadvantages too, because it restricts the choice to a relatively small number of materials. Certain properties of these materials, such as heat coefficients or fabrication ease, may not be as good as those of some other, non-

piezoelectric type; therefore, when these aspects become especially important, non-piezoelectric devices may be encountered.

2.2 Types of surface waves

Once the assumption of infinite extent for the acoustic medium is removed from the above general case, solutions take on a variety of forms, depending on the particular boundary conditions. One comparatively simple case is that of a semi-infinite solid, i.e. one with a free surface at $x_3 = 0$ in the Cartesian coordinate system of Fig. 3. If the material is isotropic and non-piezoelectric, the solution of the wave equation represents a "straight-crested" surface wave, i.e. one whose amplitude is constant all along the wavefront. The amplitude of the displacement decays exponentially below the surface. A graph of the pattern of particle displacements for this so-called Rayleigh wave is shown in Fig. 2. The individual particles have a longitudinal and a transverse velocity component, the result being an elliptical movement in the sagittal plane (i.e. perpendicular to the wavefront) [22].

The next case is that of a non-isotropic material (still non-piezoelectric). Here the phase velocity becomes dependent on the direction of propagation along the surface. The manner in which displacement amplitude changes with depth is no longer smoothly exponential, but rather takes on the form of an exponentially damped sinusoid. These waves are known as generalized

Rayleigh waves, or Rayleigh-type waves.

When piezoelectricity is introduced, non-isotropy is generally implied too, although there may exist surfaces in a piezoelectric material where isotropy prevails. Again, as in the bulk-wave case, weak piezoelectricity does not have a significant effect on the result of the analysis, but strong coupling must be taken into account. In either case the nature of the surface wave is that described in the case of the non-isotropic case above. Since strongly piezoelectric materials have such practical importance, the analysis of propagation on their surfaces is taken up in detail in Section 2.4.

Whereas the generalized Rayleigh wave is essentially illustrated by Fig. 2, another type of displacement pattern may also exist in certain piezoelectric media, referred to as electro-acoustic wave. Here the particle motion is entirely transverse to the propagation vector and also parallel to the free surface. Hence, the individual particle moves along a straight line parallel with the wavefront. The depth of penetration below the surface is greater than that of Rayleigh-type waves, but otherwise they share common properties regarding device behaviour.

Another modification of the boundary conditions is the removal of the "semi-infinite" size assumption. It leads to the case of elastic wave propagation in thin plates. These waves are called Lamb-modes. Their distinguishing features are frequency-

cutoff (i.e., depending on plate dimensions, there is a minimum frequency for propagation) and fre ency dispersion.

When the "free-surface" boundary condition is discarded we may consider the boundary of two semi-infinite media as the path for a certain type of surface wave, called "Stoneley-wave". Only a restricted number of material combinations makes propagation possible. The attractiveness of this mode lies in the possibility of isolating the propagation path from outside contamination.

Another modification to the "free surface" condition is the placement of a thin film (instead of another semi-infinite solid, as in the case of Stoneley-waves) on the surface of the substrate. The thinness of the layer is considered in terms of acoustic wavelength, which of course varies with frequency. For this reason, surface waves propagating under these conditions are frequency dispersive, i.e. their velocity varies with frequency. Different propagational modes are possible, the best known being the so-called Love-waves with particle motion resembling that of electro-acoustic waves. Another possible mode is a generalized Rayleigh-wave. The thin layer loads the substrate surface mechanically. One possibility is having a layer which is less stiff and more dense than the substrate. This type of layer is said to "load" the surface. Phase velocity in this case decreases with increasing propagation constant. An example of such combination is gold on lithium niobate. Both Rayleigh-type and Love-

modes are possible. Another possibility is a layer which is stiffer and less dense than the substrate, such as aluminum on T40 glass. A layer of this kind "stiffens" the substrate, resulting in phase velocity which increases with increasing propagation constant. Love-waves cannot propagate in a stiffened substrate, but generalized Rayleigh waves do. Such thin-film-on-thick-substrate techniques offer an opportunity to combine desirable characteristics of the film (piezoelectricity) and the substrate (small attenuation, or small temperature coefficient) [24], [33].

2.3 Analysis of surface waves in piezoelectric media

A mathematical analysis of surface wave propagation was made by Farnell [16] for a number of different crystals as well as directions within the crystal structure. The analysis is an elaborate one on account of the complexity of cases which have practical significance. The major source of this complexity is the anisotropic nature of the materials used for surface wave applications. The propagational characteristics of crystals depend strongly on the orientation of the surface with respect to the crystalline axes. Furthermore, most of the practical surface wave devices operate on the basis of piezoelectricity in order to allow direct excitation. Piezoelectricity also involves anisotropy. Consequently, particular results of the analysis are necessarily restricted to particular cuts of particular materials. No general solution in closed form is possible which would apply to all orientations of all crystals.

The starting point of the analysis is the coupled elastic wave equations for piezoelectric solids, (5) and (6). The potential ϕ also satisfies Laplace's equation outside the solid:

$$\nabla^2\phi = 0 \tag{8}$$

The above wave equations form the basis of bulk-wave, as well as surface-wave solutions, these emerging by the establishment of suitable boundary conditions. In the surface wave case, solutions are sought which resemble the known form of surface waves, i.e. they should decay with depth below the surface and should be "straight crested", meaning the displacement is independent of distance perpendicular to the plane containing the propagation vector and the normal vector to the surface (sagittal plane). Such solutions will be combinations of terms with the following form:

$$u_j = \alpha_j \exp ik\,(l_i \cdot x_i - vt) \tag{9}$$

$$\phi = \alpha_4 \exp ik\,(l_i \cdot x_i - vt) \tag{10}$$

where l_1 and l_2 are directional cosines specifying the direction of propagation, while l_3, v and the eigenvector components α are unknown and to be determined. The coordinate system for the problem is shown in Fig. 3. When this form of solution is substituted into the wave equations, a set of four homogeneous equations in the α's result, of the form:

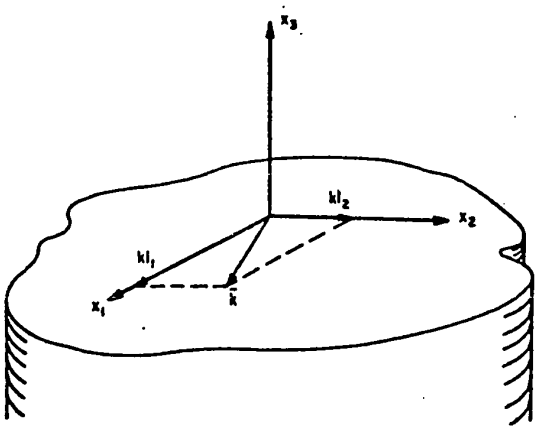

Fig. 3 Coordinate system for the surface wave problem

$$(\Gamma_{rs} - \delta'_{rs}\rho v^2)\alpha_r = 0 \qquad (11)$$

where $\Gamma_{jk} = C_{ijkl}\, l_i\, l_l \quad (i,j,k,l = 1,2,3)$

$(r,s = 1,2,3,4;\ \delta'_{44} = 0)$

Considering v as the parameter (its values are to be determined later) and setting the expression inside the brackets to zero, an eighth order algebraic equation in l_3 results, with real coefficients. The eight roots of the equation form four conjugate pairs; four roots being located in the upper half of the complex plane, four in the lower half. Those in the upper half correspond to solutions, whose magnitude increases with depth (negative x_3); being at odds with practical experience, they are discarded. The four lower-half-plane roots yield solutions of the following forms:

Displacement:

$$u_i = \sum_{n=1}^{4} c_n \alpha_i^{(n)} \exp\left[ik(l_1 x_1 + l_2 x_2 + l_3^{(n)} x_3 - vt) \right] \qquad (12)$$

Potential:

$$\phi = \sum_{n=1}^{4} c_n \alpha_4^{(n)} \exp\left[ik(l_1 x_1 + l_2 x_2 + l_3^{(n)} x_3 - vt) \right] \qquad (13)$$

which are the appropriate linear combinations of the form of solution mentioned previously, provided the values of the c's are chosen in a manner that will satisfy boundary conditions. These conditions in the piezoelectric case are the following:

$$\text{Surface traction } T_{3j} = C_{3jkl} \frac{\partial u_k}{\partial x_l} + e_{k3j} \frac{\partial \phi}{\partial x_k} \qquad (14)$$

(in contrast to the non-piezoelectric case where $T_{3j} = 0$ on the surface, i.e. at $x_3 = 0$, indicating a "free" surface)

The other boundary conditions demand that the potential must satisfy Laplace's equation above the surface, must be continuous at the surface, and decay to zero at infinite heights above the surface. This latter is satisfied by an exponential decrease of potential, a suitable form for Laplace's equation as well. The last boundary condition, that of the displacement and potential decaying to zero at infinite depths into the solid, has been built into the solution by virtue of the form of solution originally selected.

The boundary conditions form a 4x4 determinant, which, when the appropriate value of the parameter v (velocity) is substituted, becomes zero. To locate these values of v is an intricate problem, which may best be performed by a computer, using iterative search, i.e. trying out successive values of v, while the calculated value of the determinant approaches zero. Once the value of v is found, the c_n's (weighting factors) of the equations for u_i and ϕ can be evaluated, yielding the complete expressions for displacement and potential as a function of distance, depth and time.

Naturally, such expressions are applicable to one particular cut of a specific crystal. For any other case, the calculations must be repeated and in general will produce a diffe-

rent set of results.

Qualitatively, results show that the surface wave velocity in piezoelectric crystals is higher than in non-piezoelectric ones (the effect is referred to as "piezoelectric stiffening"), but in almost all cases lower than bulk-wave velocities. This latter effect may be visualized by regarding the surface of the crystal as being less restricted than the interior, consequently resulting in lower velocities. This also explains why surface waves remain on the surface: the interior cannot support waves of such low velocity. Another result shows that the manner of decay of displacement with depth is not simply exponential, but oscillatory with an exponentially decreasing amplitude.

The previously mentioned elliptical motion of the particles of the crystal is borne out by the calculations, the exact manner, orientation, being a function of crystalline direction as well as depth below the surface.

Besides the waves described which may be called generalized Rayleigh waves, the solutions point to another possible propagational method having displacements entirely transverse to the propagation vector. This wave is the previously mentioned electroacoustic surface wave. Also, in certain directions, phase velocity may exceed the lowest transverse bulk wave velocity. The result is the propagation of "Pseudosurface wave" or "leaky" surface wave, where surface wave energy is transformed into bulk-

wave, resulting in a "leaking" of energy from the surface wave. A matter of practical importance is the ability to locate those directions and surfaces of a given crystal, which will lend themselves most efficiently to the generation of surface waves. A measure of this efficiency for piezoelectric crystals is the so-called effective coupling constant, relating amplitudes of the traveling electric field and the associated elastic wave. Strong coupling is desirable for efficiently transferring electromagnetic energy to elastic surface wave energy.

A method of determining these optimum directions and cuts was developed by Campbell and Jones [9]. They evaluated the change in the surface velocity which occured when an infinitely thin sheet of conductor was placed on the surface. Such film forces the electric field to become zero above the surface without mechanically loading the surface. Calculations show that this change in velocity is related to the effective coupling constant in the following way:

$$k^2 \cong -2 \frac{\Delta v}{v_o} \tag{15}$$

where v_o is the velocity with the non-electroded surface, and k is the effective piezoelectric coefficient, a quantity proportional to the electric field at the surface when there is unit power flow in the acoustic wave [22]. In lithium niobate, the material with the strongest piezoelectric coupling, k^2 is about 0.05 under optimum conditions. The negative sign accounts for the fact that

Δv itself is negative, i.e. a decrease in velocity due to electroding.

It may be concluded that if no change in velocity occurs under the conditions mentioned above, i.e. no interaction takes place between the surface and the conducting film, the electric field must be primarily tangential. Conversely, a large normal component may be expected to produce strong coupling.

2.4 Surface wave attenuation and amplification

The losses associated with acoustic wave propagation are small compared to those of guided electromagnetic waves, when expressed in terms of loss per wavelength or unit delay, a meaningful comparison, since the main reason for the existence of acoustic devices is their low propagational velocity.

As an example, surface wave attenuation in a lithium niobate delay line for a 4 μsec delay is about 10 db at the frequency of 1.65 GHz. To achieve the same delay for a guided microwave signal, about 3600 ft of good quality coaxial cable would be required with an insertion loss of about 180 db. Furthermore, the size of the acoustic delay line in this case is about half an inch only [26]. Including the transducer losses, the total insertion loss would be in the order of 20 db. At lower frequencies, attenuation is less and, except in the case of long delay lines, becomes negligible compared to losses associated with

transduction (it is about 0.1 db/cm at 200 MHz in lithium niobate).

Surface wave attenuation is due to the following sources:

1. scattering of the coherent surface wave by thermal phonons,
2. loss due to scattering of energy at points where there are changes in material properties, such as surface cracks, elastic discontinuities at points of contact of crystallites in polycrystalline solid (strong scattering takes place as the acoustic wavelength becomes comparable to crystallite dimensions), presence of electrical discontinuities on a piezoelectric crystal,
3. surface loading; this may become a factor even when the medium adjacent to the surface is air. The transverse elastic waves lose energy to compressional volume waves in the air,
4. conversion of energy from fundamental to higher harmonics in a nonlinear medium,
5. electronic loss in a conducting or semiconducting medium,
6. losses associated with "leaky waves" i.e. conversion of part of the surface wave energy into bulk waves,
7. losses due to viscous contaminants on the surface [50], [10].

The first of this list tends to be the most significant contributor under normal circumstances, especially at high frequencies. It is also temperature-dependent due to the thermal phonon interaction mechanism.

The significance of surface cracks and contaminants also

increases as microwave frequencies are approached since their size becomes significant compared to the small wavelength of the signal. For this reason, surface wave substrates used in microwaves are carefully polished and often encapsulated. Low loss propagation can be enhanced by the use of single-crystal materials. This tends to eliminate losses due to scattering by crystallites. Single crystal substrates have the additional feature of easily reproducible properties. The uniformity of quality usually justifies the higher initial expense of using single crystals [12].

There is a practical limit to the size of a single-crystal piece of material that can be manufactured. When larger dimensions are required--for longer delays as an example, one possibility of extending the effective length of the crystal offers itself for piezoelectric materials. As shown in Fig. 4, the electric field associated with the traveling surface wave in the crystal on the left extends above the surface. Another piece of crystal is placed next to the first one, with an area of overlap. The two crystals are separated by an air gap with a width in the order of one acoustic wavelength. The electrostatic field transfers acoustic energy across the air gap onto the under-surface of the second crystal. Reflections from the end faces of the crystal blocks can be prevented by a suitable coating of absorbing material such as wax.

An aspect of the acoustic path often more important than the value of attenuation or velocity of propagation is the cons-

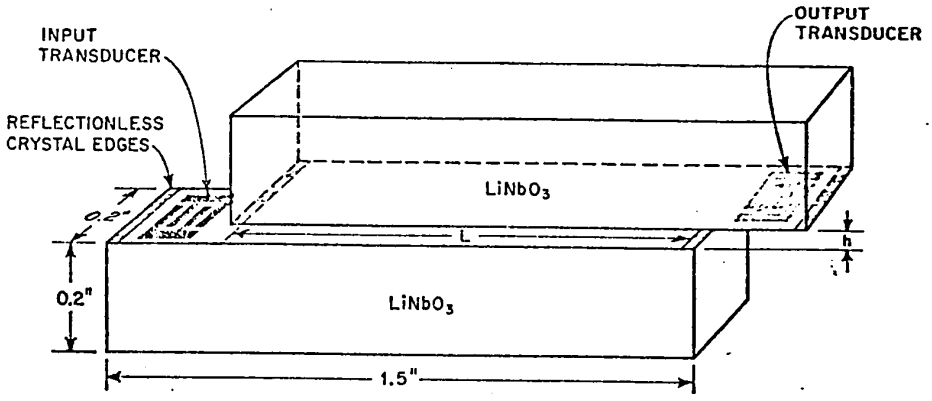

Fig. 4 Piezoelectric coupling through a gap

tancy of these factors in terms of temperature. While the choice of materials is restricted to the few reasonably strong piezoelectric substances, one must accept the temperature characteristics of these. A later trend, however, endeavors to combine the best characteristics of the piezoelectric transduction and thermal stability of certain non-piezoelectric substrates.

An example of this is the use of isopaustic glass as the substrate with the excellent stability of delay constant of 6 parts in 10^6 per degree centigrade over a -30°C to 80°C range [33]. A piezoelectric film covers the area where the transducers are located. The electrical input generates an acousto-electric wave in the film which in turn couples over into the bare substrate as a purely acoustic signal. Transducer arrangement for this type of device is mentioned in Section 3.1.

Considering the propagation losses and the inevitable transducer losses, acoustic devices can represent a sizeable insertion loss in a circuit, one that may become prohibitive for delay lines of long delays or high fequencies [22].

Another problem arising from transducer operation, as will be discussed in Chapter 3, is the reflection of acoustic waves from the transducers. Such reflections give rise to echoes, a measure of which is known as triple-transit echo. This is a delayed version of the original output signal, arriving at the output after being twice reflected, once at the output, and

once at the input transducer. Generally it is difficult to achieve an echo level more than 20 db below the required signal, which is an unsatisfactory figure for many applications.

The solution to the above problems is the construction of a nonreciprocal acoustic device with amplification. The use of an internal, rather than an external amplifier has the advantage of increased dynamic range. The minimum signal amplitude is limited by the noise of the delay-line-amplifier system, the maximum amplitude by the saturation power of the acoustic device. While an internal amplifier frees the full dynamic range of the system, with an external amplifier this range is decreased by the delay-line loss. Since amplifier action is non-reciprocal, triple transit suppression (TTS) of better than 40 db can be obtained. Such internal amplifiers have been built, first for bulk waves [12]. The bulk medium was a piezoelectric semiconductor such as cadmium sulfide. A d-c electric field is applied to the substrate, causing electrons to drift through the device parallel with the direction of propagating acoustic waves. In a manner similar to that of traveling wave tubes, interaction between drifting electrons and the electric field component of the acoustic wave takes place. If the drift velocity exceeds that of the acoustic wave, kinetic energy of the electrons is converted to r-f energy. Sizeable gains in the order of 60-80 db/cm are possible.

The bulk material must have the following qualities: strong piezoelectricity, low acoustic attenuation and efficient

semiconduction . Unfortunately, no single substance possesses all three qualities to a satisfactory degree. An answer to the problem is provided by surface wave acoustic amplifiers. The most frequently used type [50] operates in a manner similar to the device of Fig. 4. A semiconductor layer is situated above the acoustic substrate, separated by a narrow air gap as illustrated in Fig. 5.

Drifting electrons in the semiconductor layer interact with the acousto-electric wave in the lower substrate through the electric field of the latter extending across the gap. In a construction of this type, the semiconductor and acoustic media are separate, therefore the optimum choice of materials can be made for both. Another configuration of the amplifier utilizing the same interaction between Rayleigh waves and drifting electrons is the monolithic amplifier. This construction eliminates the air-gap (often the source of difficulties) and replaces it with a thin layer of dielectric material such as SiO [11].

While piezoelectric-semiconductor amplifiers are the ones most commonly used, other types are also being investigated; among them parametric amplifiers, utilizing nonlinear interaction of acoustic waves. Such nonlinearity arises at power levels which are sufficiently high to cause stresses no longer proportional to the strains [22]. As an example, at approximately 1 watt of acoustic power, a 100 MHz surface wave device with a beam width of 1mm and a penetration depth of 5 μm will develop

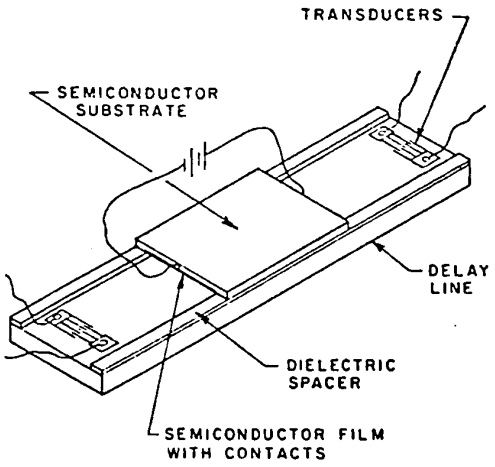

Fig. 5 Acoustic surface wave amplifier

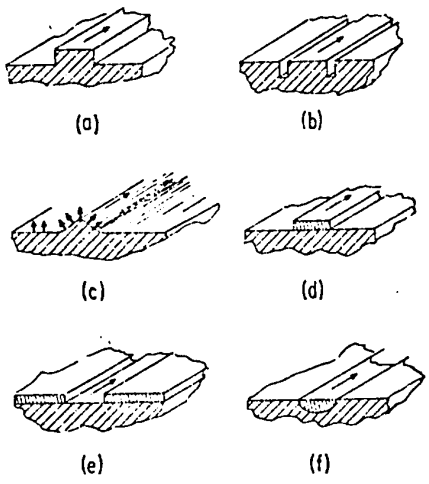

Fig. 6 Surface waveguides

a strain (relative displacement) of 10^{-3} which is already well above the limit at which Hooke's Law of linearity applies. Such nonlinearity holds the promise of parametric amplification, with two inputs and an output along the lines of electronic models and their signal, pump and idler frequencies.

2.5 Guiding of surface waves

The ability to control the direction of the path surface waves take is an important aspect of constructing acoustic devices [2], [12], [32], [50]. The acoustic beam emerging from transducers is usually wide and spreading as it proceeds. As a result, some of the propagating energy misses the receiving transducer. By confining the traveling energy to a narrow channel, better utilization of the acoustic medium is possible. For example, delay lines can be built with serpentine paths, hence long delays in a small area. If acoustic devices are to fulfill their promise in compact integrated circuit applications, means must be found to confine the lateral spread of the acoustic beam to a few wavelength's width.

A number of methods have been proposed, some of which are illustrated in Fig. 6. The principle of guiding in all these cases is either the confinement of the signal by reflections from the sidewalls of a channel, or the creation of a path where the phase velocity of the wave is less than in the surrounding medium. In Figs. 6(a) and 6(b) (ridge guide and channel guide, respectively)

for example, the designated path is surrounded by a free unrestrained wall on both sides: less restraint leads to lower velocity and the concentration of the energy into the channel. Fig. 6(c), showing topographic guiding is closely related to them.

The other group of guiding schemes involve two different materials, the substrate and a thin film overlay. This is a promising method which makes use of available technology in deposition techniques. Fig. 6(d) shows the use of a stripe of material more massive but less stiff than the surrounding substrate. This "slow-on-fast" structure confines energy to the stripe because of the lower velocity there. Since velocity is inversely proportional to the square root of density, slow overlay materials generally have higher density than the substrate. A similar way is indicated in Fig. 6(e), a "fast-on-slow" guide. In this case the coating material is less massive but stiffer than the substrate resulting in a higher velocity outside the exposed substrate channel. Again, energy is confined to the slow region.

At high frequencies, where single crystal materials are desirable, epitaxial deposition is used. For piezoelectric substrates, the slow path may be provided by a thin layer of metal. Its presence removes the "stiffening" effect of the piezoelectric field from the region covered, thereby allowing a lower phase velocity. Fig. 6(f) shows a guide having a low-velocity center section

fused or grown into the faster substrate. It shares the properties of the models of Figs. 6(d) and 6(e), being a combination of two materials.

A fundamental feature of guiding is the introduction of frequency dispersion. This is seldom deliberate or desirable, because dispersion may be achieved more conveniently with appropriate transducers (see Chapter 3). The reason for the dispersion is the variable depth of penetration as a function of frequency. In the presence of a film overlay, different frequencies are delayed to different extents. Dispersion is also affected by the curvature of bends. Unlike electromagnetic waveguide bends, acoustic guide bends involve appreciable loss due to radiation out of the guide. If appropriate measures are taken in the construction of guides, variations can be held to quite acceptable limits. One such technique is the tapering of the thickness of the overlay film in bends. Typical values are a velocity change of 5% for a frequency change of a factor of 2.5, a right-angle bend of 100 wavelength radius, resulting in a loss of 1.5 db at 10 MHz [12].

Another method of directing acoustic waves along curved paths or focusing acoustic energy into specific regions is through acoustic lenses. The most attractive method involves a suitably shaped film material deposited on the surface. By delaying portions of the passing acoustic wavefront according to the distance they travel under the film, any desired wavefront configuration can be achieved, in a manner analogous to optical

lenses. Focusing can also be arranged by appropriately shaped transducers (see Section 3.5). Fig. 7(a) illustrates a focusing lens made out of a conducting electrode on a piezoelectric surface; Fig. 7(b) shows the manner in which surface waves can be guided around a bend with the help of lenses [50].

Still another method of changing the direction of surface waves is by reflection. As in all other forms of wave propagation, discontinuity in path characteristics will result in part of the signal energy being reflected. While in many cases this is an undesired effect involving energy losses and echoes, it can be harnessed to produce the necessary changes in direction. Controlled reflections in piezoelectric materials can be produced by arrays of conducting stripes whose elements are either isolated from one another or connected through reactive or active circuit elements [50]. Direction of the reflected signal is determined by the orientation of the array elements.

A sophisticated method of reflecting acoustic surface waves is described by B.A. Auld et al [4]. Fig. 8 shows the physical arrangement consisting of YZ-cut lithium niobate substrate and interdigital transducers. In the center, a thin layer of CdS is evaporated onto the surface. The CdS film is photoconductive, therefore light incident on it produces photoconductive carriers. These in turn can interact with the acoustoelectric surface wave propagating along the piezoelectric substrate. Using laser beam illumination, the illustrated optical

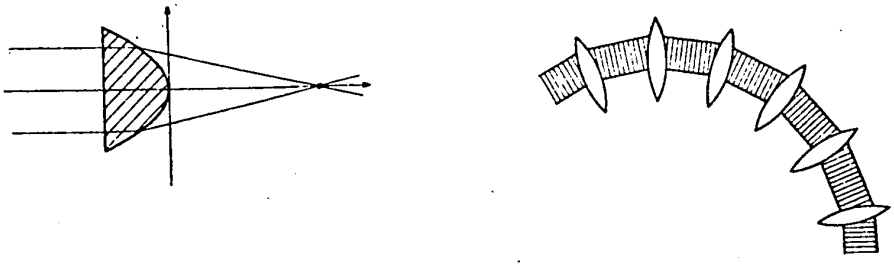

(a) (b)

Fig. 7 Acoustic lenses

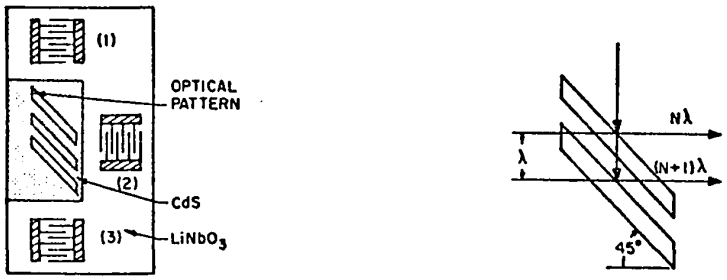

Fig. 8 Optical reflection of surface waves

pattern can be created. Due to the appearance of carriers in the areas involved, surface impedance changes abruptly, resulting in reflection. With suitably chosen periodicities, reflection from each band will add constructively. In the setup shown, signals emitted from transducer (1) are reflected towards (3). Removal of the illumination results in undisturbed propagation from (1) to (2). The technique is a versatile one, being also capable of generating, detecting and attenuating surface waves. It will be taken up again in Section 3.1 under transducer types.

CHAPTER 3

SURFACE WAVE TRANSDUCERS

3.1 Surface wave transducer types

Transducers are the means of conversion between electric and elastic energies, i.e. the launching and reception of acoustic waves. This report deals with surface wave transducers only, omitting bulk wave devices. Within this class, too, there is an extensive variety of transduction schemes, each having particular features that may make it attractive for a given application [43], [50].

Surface wave transducers may be classified into two groups, operating on the following principles:

(a) mode conversion from bulk to surface waves

(b) generation of suitable stresses near the surface of a solid

In group (a) one can find some of the early device models such as the wedge transducer of Fig. 9 and the comb transducer of Fig. 10. In the wedge model, bulk waves originate in the bulk transducer, and propagating down into the wedge, couple over onto the surface. The resulting surface waves propagate towards the right hand side. The angle of the wedge is selected in such a way that the bulk wavelength measured along the contact surface equals the surface wavelength. Reflected bulk waves are absorbed by a layer of suitable material.

A more efficient model is the comb transducer. Its teeth

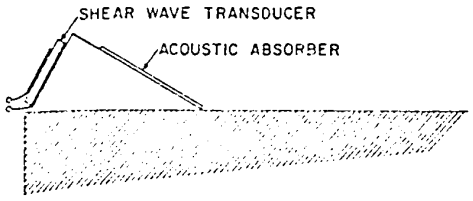

Fig. 9 Wedge transducer

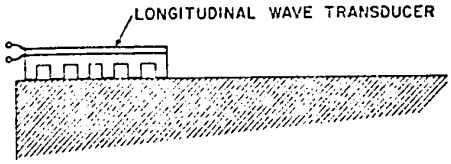

Fig. 10 Comb transducer

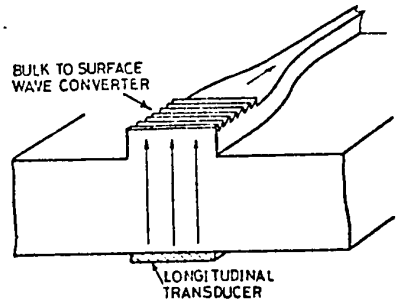

Fig. 11 Corrugated transducer

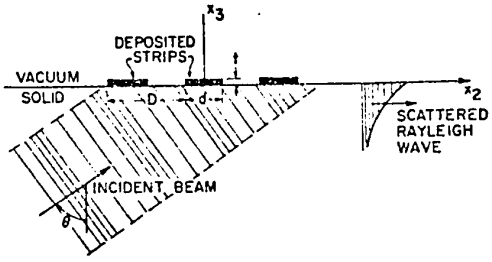

Fig. 12 Bulk wave to surface wave conversion

are set one Rayleigh wavelength apart. The longitudinal bulk wave moving down from the transducer on top, couples to a standing wave on the surface, radiating an acoustic surface wave to the left as well as to the right. Energy also radiates downward into the bulk of the substrate.

Figures 11 and 12 show two other methods of bulk wave to surface wave conversion [2]. The corrugated transducer of Fig. 11 is illustrated here in one of its applications, as terminating apparatus for an acoustic surface waveguide. Upward radiating bulk waves are partially converted into surface waves when groove period equals surface wavelength and wavelength of bulk wave projected onto surface. The asymmetry of the grooves favors one direction of surface propagation.

Bulk wave scattering is also the mechanism in Fig. 12 [7]. The bulk wave beam is incident on infinitely long metallic strips deposited on the surface. When the angle of incidence satisfies the usual conditions, surface wave excitation results, due to the mechanical motion of the strips. If the surface is piezoelectric, an additional electrical contribution to the wave will be made, due to the conductivity of the electrodes. Bulk wave conversion is generally less efficient than the direct generation of surface wave, on account of losses due to energy remaining in bulk form. For this reason they are seldom used, although some research still continues into better constructions. In a paper at the 1971 IEEE Sonics, Ultrasonics Symposium, H.L. Bertoni and T. Tamir reported

80% coupling efficiency achieved with a particularly designed wedge transducer.

In group(b) of our transducer classification, one finds the most generally used surface wave transducers. The largest and most important class among these is that of surface electrode arrays. The remainder of Chapter 3 deals with these arrays; Section 3.2 discusses the basic principles of operation as well as basic array configurations. The typical electrode array, as it appears in Fig. 13, operates by producing a spatially non-uniform, time-varying electric field pattern. When placed on a piezoelectric substrate, this field pattern will generate an acoustic surface wave through the electro-elastic action of piezoelectric materials. The transducer elements are metal electrodes forming a pattern which is deposited on a crystal surface by standard photolithographic methods or special optical techniques as discussed in Section 4.2.

A few other transducer types of group(b) merit description before going on the the detailed treatment of electrode arrays on piezoelectric substrates.

A transducer which is essentially an electrode array, but also suitable for non-piezoelectric substrates, is illustrated in Fig. 14. In this device, described by C.P. Sandbank et al [33], the substrate is non-piezoelectric. The metal electrodes are covered by a thin piezoelectric overlay of ZnO, and the signal is

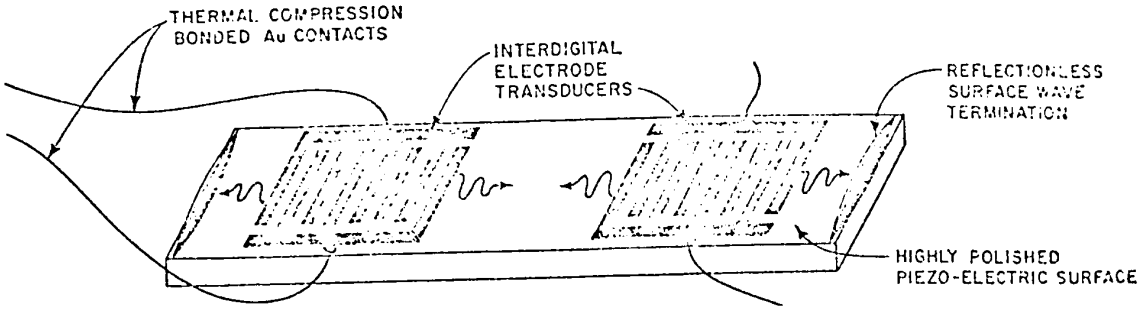

Fig. 13 Electrode array

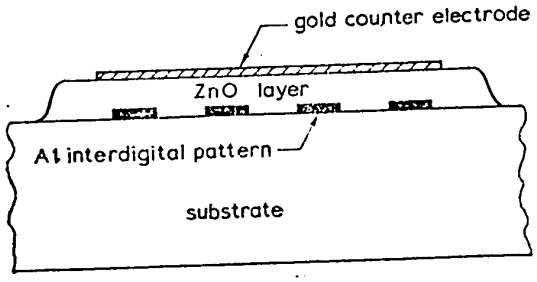

Fig. 14 Piezoelectric transduction on a glass substrate

applied between the electrode strips and the counter electrode. The electroacoustic wave generated in the ZnO layer is coupled over into the substrate (in this case isopaustic glass with excellent temperature stability) where it continues in the form of an acoustic surface wave without the electric field component. As mentioned in Chapter 2, this scheme makes possible the use of materials with attractive characteristics as substrates, and yet retain the efficiency of piezoelectric transduction.

Another transducer, which is more remotely related to electrode arrays is the photoconductive transducer, described by B.A. Auld et al [4]. Whereas in the case of the arrays, a spatially periodic electric field is applied to a piezoelectric substrate interacting with a synchroncus acoustic wave, in the photoconductive device, the same type of spatially periodic field can be produced by applying a uniform electric field to a periodically illuminated photoconductive film on the surface of the piezoelectric substrate. The arrangement is as shown in Fig. 15. A propagating Rayleigh wave as represented by the sine wave in the diagram has electric field components whose alternating directions are illustrated by the arrows. In the illuminated regions, the generated photoconductive carriers tend to short out the electric field, while the field is unaffected in the dark areas. In this manner the presence of metal strips is simulated by the illuminated regions. A net field (varying sinusoidally at the acoustic frequency) results from the addition of the fields in the dark

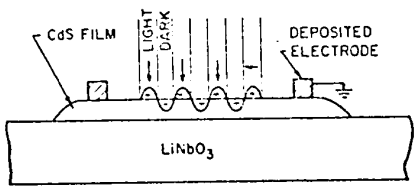

Fig. 15 Photoconductive transducer

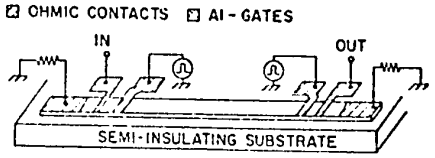

Fig. 16 FET transducer on GaAs

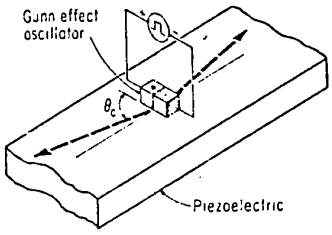

Fig. 17 Transduction through Gunn-effect

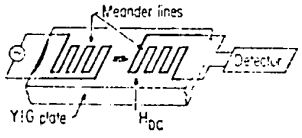

Fig. 18 Magnetostrictive transducer

regions and is sensed by the two electrodes. While the scheme is more complicated and less efficient than the electrode array, it has the advantages that the pitch of the light pattern can be varied as desired, thereby tuning the frequency of the transducer, and also the position and orientation of the pattern can be shifted easily; an advantage in variable delay line applications.

More exotic devices utilize field-effect transistors on epitaxial GaAs (Fig. 16), Gunn-effect oscillators on piezoelectric substrates and magnetostrictive transduction on YIG plate (Fig. 18)

The circuit of Fig. 16 utilizes a piezoelectric semiconductor, GaAs, which connects, in the form of a ridge, two FET's [8]. When an r-f signal is applied at the first gate, surface waves propagate down the ridge, to be detected at the second gate. The action is based on piezoelectric coupling between the acoustic waves and the current modulation in the FET's. While this coupling is weak, the gain of the FET's and the possible application of a drift field along the ridge should compensate for this.

In the device of Fig. 17, the coupling to the piezoelectric surface wave is accomplished through the electric field of the Gunn domains moving periodically through the oscillator block. The acoustic waves emerge at an angle determined by the ratio of acoustic and domain velocities [27].

Fig. 18 shows a transducer whose operation is based on magnetostriction. This is a magnetic equivalent of a piezoelec-

tric device, with a substrate of ferrite crystal (yttrium iron garnet in this case). If a spatially periodic variation of r-f magnetization is created at the surface, elastic waves will be excited. The excitation comes from r-f currents flowing in the evaporated aluminum meander lines. A static magnetic field is also applied whose orientation determines the type of surface waves generated [45].

3.2 Electrode arrays

A schematic layout of a typical transducer connection is seen in Fig. 19. The alternating voltage impressed on the electrodes interacts with the piezoelectric substrate and produces two acoustic waves which start traveling in opposite directions along the crystal surface. Although a single electrode pair is acceptable, an array of elements will result in increased efficiency. The individual elements are spaced in such a way that the surface waves they produce will combine coherently. The operation of such an electrode array is analogous to that of an electromagnetic antenna array--an end-fire array in particular. The relationship between the performances and characteristics of an individual dipole and a dipole array will also appear in the case of a transducer array, i.e. increased efficiency, directivity, decreased bandwidth, input impedance etc. In this configuration, as transmitting transducer, the device represents a load on the driving generator, with an impedance determined by the dimensions of the transducer. The matching network performs the obvious function

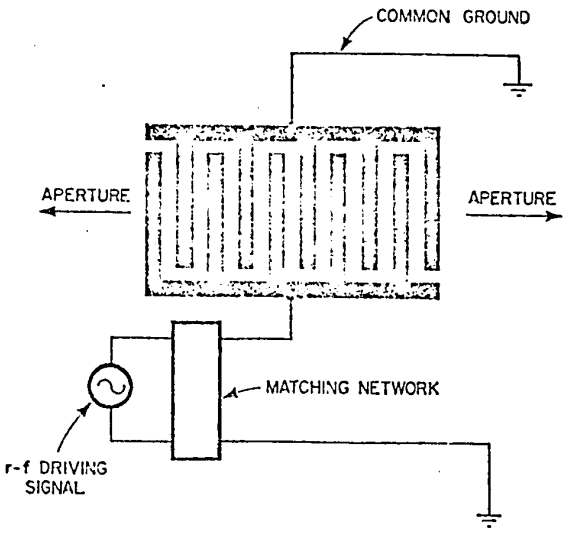

Fig. 19 Transducer circuit

of matching the impedance of the transducer to that of the generator. In a simple case, this may amount to tuning out the reactive part of the load, as it is discussed in more detail under "Transducer Analysis", Section 3.3.

In further analogy to antenna arrays, a transducer array is also a reciprocal device, equally capable of acting as a receiver of acoustic surface waves.

Besides the basic functions of launching and receiving acoustic signals, transducers perform a variety of other circuit roles, such as focusing, reflecting, coding, mixing and shaping surface wave signals. These will be treated in detail under "Variations of the Basic Array", Section 3.5.

The design of transducers for a specific application involves the selection of the crystal medium, the number of elements in the transducer array and the length of its "fingers"; knowing the operating frequency, one can determine the electrode spacing, impedance, bandwidth, necessary tuning elements, etc., according to the methods explained in "Transducer Design", Section 3.4.

Transducer arrays may be grouped into the following three basic configurations:

1. Single-phase electrode array
2. Interdigital electrode array
3. Grating array

1. Single-phase electrode array

A sketch of this configuration is shown in Fig. 20 [50]. The array consists of a set of finger-like electrodes, all at the same potential relative to the ground plate, connected to the underside of the piezoelectric slab. The electric field in the vicinity of the electrodes is shown in Fig. 20(b). The horizontal component of the field changes direction twice in each spatial period. In order to build up maximum acoustic power, the surface wave should receive an in-phase energy boost at each electrode. This happens at the frequency for which the period of the array equals the acoustic wavelength under the array (at fundamental frequency operation).

An important aspect of all these configurations is their efficiency, i.e. the acoustic power they can generate for a given electrical input:

$$\text{efficiency} = \frac{\text{acoustic power generated by transducer}}{\text{maximum power available from voltage source}}$$

The following expression affords a comparison of various electrode configurations in terms of relative efficiencies:

$$E_f = \eta GQ$$

where E_f is the efficiency, η is a measure of material effectiveness, depending on the properties of the crystal medium, G is the measure of the relative effectiveness of the electrode configura-

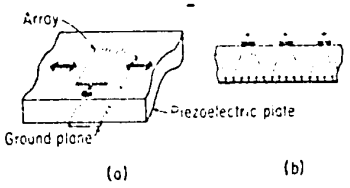

Fig. 20 Single phase electrode array

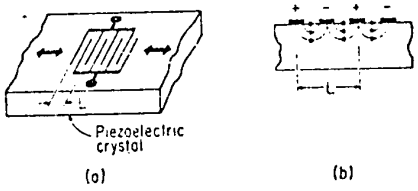

Fig. 21 Interdigital electrode array

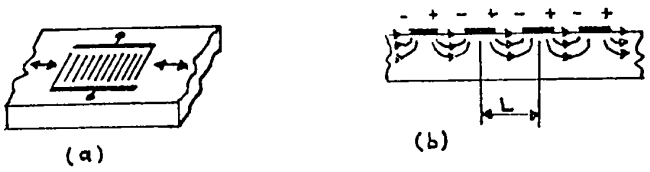

Fig. 22 Grating array

tion, and Q is the quality factor of the electrical termination. The value of G depends on the degree of similarity between the electric field of the electrodes and the electric field associated with the traveling acoustic wave. The more closely the two match, the more efficient the generating process becomes.

The major disadvantage of the single-phase array is its relatively poor efficiency compared to the other two types. Its advantages include a larger input voltage rating, due to the fact that the crystal separates the electrodes from the ground plate. A further advantage compared to the interdigital array is the wider spacing between electrodes for a given frequency. This is an important feature at high frequencies where fabrication difficulties are a limiting factor.

2. Interdigital electrode array

This is the most widely used configuration, because of its high efficiency and also because only one crystal surface needs to be prepared unlike in the case of the single-phase array, where two surfaces had to be treated. Fig. 21(b) shows the approximate electric field configuration for the interdigital array. It is apparent that two electrodes are required per acoustic wavelength. The transducer shown in Fig. 21(a) is a simple model. More elaborate versions exist, performing a variety of functions, such as pulse compression, focusing or coding. The operation of this configuration is the subject of the detailed analysis in the next section.

3. Grating Array

This array type is a recent development, reported by A.J. Bahr et al [5]. It appears to combine many of the attractive characteristics of both single phase and interdigital arrays. A sketch of this configuration is shown in Fig. 22. As seen in Fig. 22(a) the transducer is a planar array of thin metal electrodes, where only the two terminal fingers are connected to the driving source. The applied voltage produces an electric field across each gap, due to the capacitance between adjacent electrodes. Fig. 22(b) illustrates the in-phase nature of these fields (this assumes that the length of the array is small compared to the electromagnetic wavelength of the applied signal, a condition usually satisfied). If the spacing between the electrodes equals the acoustic wavelength, cumulative generation of surface waves will result. As in the case of the single-phase array, the spacing of the electrodes is λ, an advantage over the required $\lambda/2$ spacing of the interdigital array under similar circumstances. One important difference when compared to single-phase arrays is that the potential on each of the fingers of the grating array is different. In case of the uniform array, the total applied signal voltage is divided into as many equal increments as the number of elements minus 1. This division of the total potential results in an increased power-handling capability from the point of view of voltage breakdown. The grating array also shares one particular advantage of the single-phase array: a short circuit between adja-

cent fingers (which can easily occur at high frequencies where the spacing is extremely narrow) does not prevent the transducer from operating. Small breaks in the fingers are also tolerable, except in the two outside ones. Its characteristics regarding input impedance, conversion loss and ease of manufacture will be mentioned alongside the same characteristics of interdigital transducers, as the latter type is analyzed in detail in the following sections.

Finally, experimental results indicate that the efficiency of the grating array is comparable to that of the interdigital array. The sum of all these features seems to promise a successful future to this new type of transducer array.

3.3 Transducer analysis

The analysis of electrode array transducers must by necessity involve approximations. While the complexity of the field distribution calls for highly complicated treatment, practically manageable results will come only after simplified models have been substituted for the actual situation. A suitable model must, of course, account for the basic characteristics of the device and depending on its sophistication, describe some of the secondary effects occurring in transducer operation [19].

These effects include:

1. electro-acoustic regeneration on account of energy cycling between electrical and acoustical fields in the region of electrodes,

2. multiple transit reflections between input and output transducers,
3. acoustic reflections due to path discontinuity at the electrode edges,
4. spurious bulk mode signals,
5. wave diffraction and beam steering which are a function of transducer geometry and crystal substrate properties;

A number of different models have been put forward. Some, such as the elementary model of R.H. Tancrell and M.G. Holland [44] which represents the electric field gradient as δ-functions at electrode edges (see Fig. 23), are first order approximations only and cannot fully account for the secondary effects listed above.

Other models, such as the one proposed by Engan [15], are quite rigorous, but the results are in a form too complex for convenient use in the design of practical transducers.

A suitable compromise between rigor and convenience is the type of equivalent circuit first presented by W.P. Mason in "Electromechanical Transducers and Wave Filters" (Van Nostrand, 1948). His model was adapted for surface wave interdigital transducers and used successfully by W.R. Smith et al [39], [41], W.S. Jones et al [19], and C.S. Hartmann et al [18]. The model substitutes a purely electrical equivalent circuit for the transducer, with circuit elements expressed in terms of known acoustical properties.

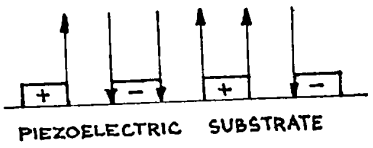

Fig. 23 Approximate electric field at transducer

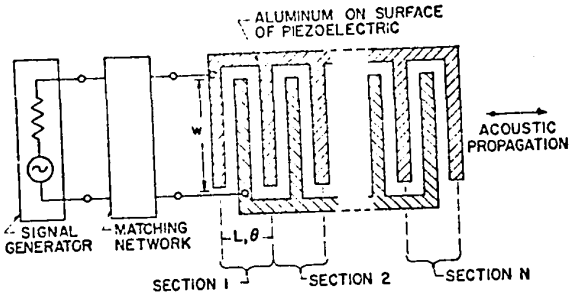

Fig. 24 The interdigital transducer

A different approach to the solution of the problem of transducer operation is represented by the work of Auld and Kino. Instead of network theory which is the basis of the following discussion, their Normal Mode Theory employs the methods of field theory [3]. The approach is the same used in electromagnetic theory to solve certain problems where exact solutions are out of reach. The normal mode expansion technique resembles the expansion of a function in terms of a Fourier series, in that one determines the possible propagational modes in the absence of a perturbing element such as a transducer, then employs these modes to express the actual conditions in terms of the original modes and the boundary conditions imposed by transducer geometry, etc. The method is used to calculate the impedance of the interdigital transducer, and yields results which are in excellent agreement with experiments. The same techniques may be applied to other acousto-electric problems, such as determining the properties of a surface wave amplifier [21].

In the following, an analysis is presented of the characteristics of the uniformly spaced interdigital transducer array. The approach is based on circuit theory, according to the work of W.R. Smith, et al [39]. While the results apply to this particular transducer type, the general approach is valid for other types too, as seen in Section 3.5.

The aim of the analysis is to develop expressions for the input admittance, scattering, electroacoustic conversion and fre-

quency characteristics of the transducer, operating on a piezoelectric substrate.

Fig. 24 shows a schematic diagram of the interdigital transducer. When a signal voltage appears across the transducer, an electric field distribution is formed between the electrodes as illustrated in the previous section, Fig. 21(b).

A rigorous solution starting with such a two-dimensional distribution becomes difficult to attain. On the other hand, solutions that have excellent agreement with experiments can be obtained based on simplified, one-dimensional models of the electric field. Fig. 25 shows the actual distribution and two possible one-dimensional representations of it. While the actual field is never quite so simple as either Fig. 25(b) or Fig. 25(c), in most cases it resembles one or the other to a sufficient degree that the simplification may be made. Whether the cross-field or the in-line field is the better representation of a particular case depends on the medium and the crystal cut; it can be determined by calculation of the stored coupling energy by the two field components. Whichever energy contribution dominates, will point to the appropriate model to use [42].

The one-dimensional model makes possible the representation of the elementary transducer by an equivalent circuit, as in Fig. 26. The diagram illustrates the cross-field model; for the in-line model, the $-C_s/2$ capacitors are short-circuited. The cir-

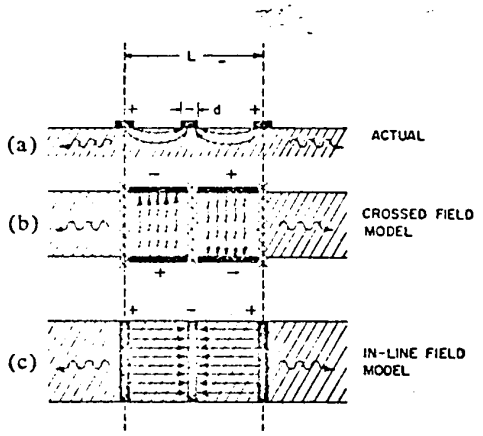

Fig. 25 Simplified field distributions

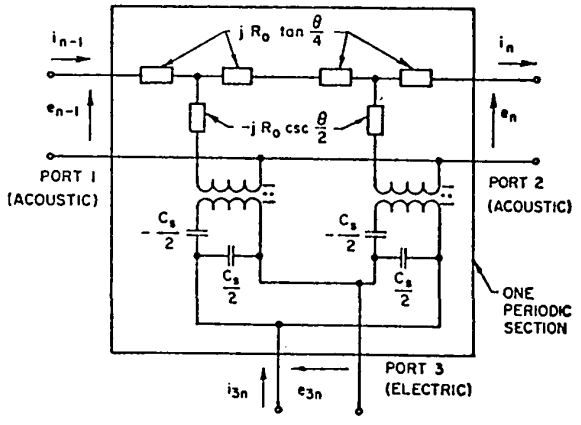

Fig. 26 Equivalent circuit of elementary transducer

cuit enables one to represent the transducer in purely electrical terms from the point of view of the connecting circuit. It indicates that the device is a three-port unit, and a symmetrical one regarding the two acoustical ports. This shows that the transducer under consideration radiates elastic waves equally in both directions perpendicular to the electrodes.

The equivalent electrical quantities at the acoustic ports represent acoustic quantities of course, with the following relationship existing between them:

$$e_i = F_i/r \qquad i_i = U_i/r$$

where F_i = acoustic terminal force

U_i = particle velocity

r = turns ratio of acoustic-to-electric transformer =

$= hC_s/2$

where h = piezo constant

C_s = electrode capacitance/period

Other quantities in Fig. 26 are defined as follows:

$$R_o = \frac{Z_o}{r^2} = \frac{2\pi}{\omega_o C_s k^2} = \frac{1}{f_o C_s k^2}$$

where Z_o = substrate mechanical impedance = $Av\rho$

k = electromechanical coupling constant

R_o = electrical equivalent of Z_o

$\omega_o = 2\pi f_o$ = synchronism frequency

$f_o = v/L$ = sound velocity/periodic length

$\theta = 2\pi\omega/\omega_o$ = periodic section transit angle

ω = source frequency

A = cross sectional area

ρ = density

The three quantities that are to be specified to describe the equivalent circuit are: f_o, C_s and k. Of these, f_o is determined from v/L, velocity being known for the various crystalline orientations. C_s can be determined from the dimensions of the transducer and the dielectric properties of the crystal, while k may be obtained by a procedure mentioned previously, where it may be visualized, that the substrate surface is covered with an infinitesimally thin metal layer. Being thin, the layer does not load the surface mechanically, i.e. it does not interfere with the elastic displacement, but being a conductor, it eliminates surface charge. The acousto-electric properties of the substrate thus changed, the surface velocity will change by a certain amount compared to the non-electroded case. The extent of this change is a measure of electromechanical coupling, with the already mentioned specific (but approximate) relationship:

$$\frac{\Delta v}{v} \cong - \frac{k^2}{2} \qquad \text{(equation 15 in Section 2.4)}$$

This procedure can be realized experimentally as well, and the results verify the above relation. The relationship is an accurate one for bulk waves, but for surface waves, often a multiplying

constant called filling factor (F) is employed to make the equation more accurate:

$$\frac{\Delta v}{v} = - Fk^2$$

where F is generally 1 ± 0.2 depending again on transducer configuration.

In an actual surface-wave device, such a metallic layer does exist, in the form of the transducers themselves. They amount to a partial overlay of a very thin conducting layer. Such a layer would naturally change the characteristic impedance of the medium, hence under the transducer one finds a region with periodically alternating areas of different Z_o [41]. The transducer fingers are usually thin enough not to load the surface mechanically, so the major cause of the impedance discontinuity is the shorting of the tangential electric field by the metallic electrodes. Because of the two different characteristic impedances, there will be two different surface velocities as well, for the two regions. We can designate them as: v_m, Z_m for the electroded regions, v_o, Z_o for the non-electroded regions. The corresponding transit angles are:

$$\Psi = 2\pi f L_s / v_m \qquad \text{and} \qquad \phi = 2\pi f L_g / v_o$$

The total transit angle is $2[\Psi + 2\phi]$, corresponding to Θ in Fig. 26. The equation for the synchronous frequency becomes:

$$f_o = \frac{1}{2}\left[\frac{L_s}{v_m} + \frac{L_g}{v_o}\right]^{-1}$$

T · equivalent circuit of Fig. 26 may be redrawn to include the acoustic impedance discontinuity. Unlike Fig. 26 which depicts one complete section, Fig. 27 represents a single electrode unit as L/2 in Fig. 27(b).

The effect of the impedance discontinuity on the operation of the transducer is to introduce acoustic reflections at the electrode boundaries, creating echoes and degrading the triple transit suppression of the device.[1] Another effect is the introduction of some directivity into the transducer, which was so far regarded as a symmetrically two-way device from the acoustical point of view. The measure of the impedance discontinuity

$$\tau = \frac{Z_o}{Z_m} = \frac{v_o}{v_m} = \frac{v_m - \Delta v}{v_m} = 1 - \frac{\Delta v}{v_m} = 1 + \frac{1}{2}k^2$$

shows that it is proportional to the electromechanical coupling constant, hence it varies with the crystal material and cut.

Since the reflection coefficient is quite small even for strongly piezoelectric cases, in short arrays the above effects

---

[1]This quantity (TTS) compares the level of the first multiple reflection echo with the desired signal:

$$\text{TTS (db)} = 2\,(L_{11} + L_a)$$

where L_{11} = reflection loss at transducer

L_a = propagation loss, one way

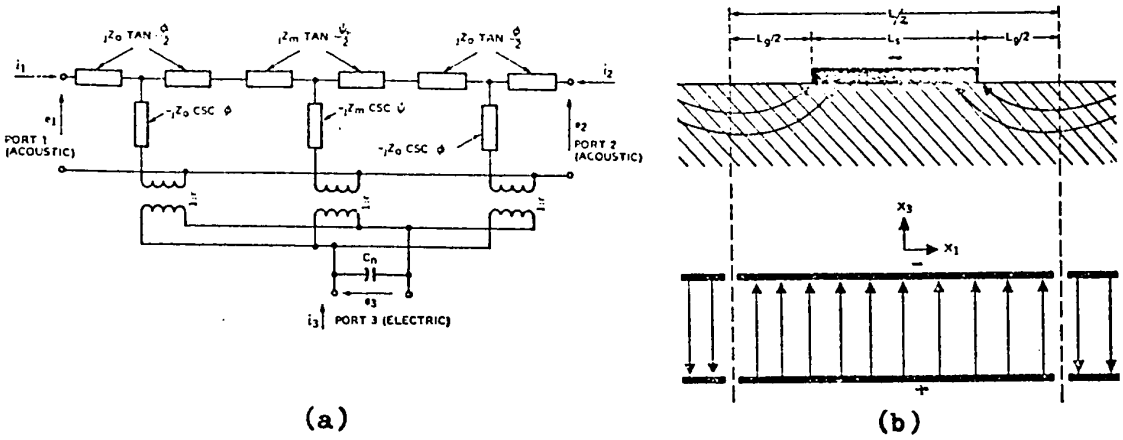

Fig. 27 Equivalent circuit allowing for electrode mismatch

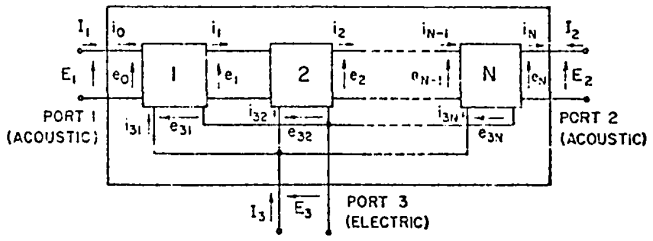

Fig. 28 Equivalent circuit of complete array

are generally small, and may be neglected. In arrays of a 100 or more electrodes however, the reflected signals combine coherently, and ignoring the effect of discontinuities leads to altogether erroneous results. A quantitative analysis including the above effects has been put forward by W.R. Smith et al [41].

As will be seen shortly, uniformly spaced transducers (the topic of this section) are made up of relatively few transducer sections, usually less than 20. Hence, the effect of discontinuities will not be necessary to include in the subsequent analysis, but should be considered in the design of certain special transducers.

The complete transducer of N periodic sections is represented by its equivalent circuit in Fig. 28. From the acoustical point of view, the individual sections are in cascade, in the manner of an end-fire antenna array. Electrically, however, they are in parallel.

A significant difference appears here between the interdigital and the grating arrays: in the latter, the sections are electrically in series. Consequently, the grating array may present a large input impedance, often an advantage.

The transducer equation, based on Fig. 28, may be written as:

$$\begin{bmatrix} I_1 \\ I_2 \\ I_3 \end{bmatrix} = [Y] \begin{bmatrix} E_1 \\ E_2 \\ E_3 \end{bmatrix} \quad \text{where} \quad [Y] = \begin{bmatrix} Y_{11} & Y_{12} & Y_{13} \\ Y_{12} & Y_{11} & -Y_{13} \\ Y_{13} & -Y_{13} & Y_{33} \end{bmatrix}$$

The $[Y]$ matrix reflecting the symmetry of the transducer regarding the acoustic parts. The Y_{ij} terms can be determined from Figs. 26 and 28. For the sake of brevity, the results shown here correspond to the case of acoustic synchronism and the adjoining frequency band (the more general case is also treated by W.R. Smith et al [39].

For the "in-line" model:

$$[Y] = \frac{j\omega_o C_s}{16} \begin{bmatrix} -\frac{1}{N} & \frac{1}{N} & 4 \\ \frac{1}{N} & -\frac{1}{N} & -4 \\ 4 & -4 & 0 \end{bmatrix}$$

For the "crossed-field" model:

$$[Y] \cong \frac{jG_o}{\delta} \begin{bmatrix} -\frac{1}{N} & \frac{1}{N} & 4 \\ \frac{1}{N} & -\frac{1}{N} & -4 \\ 4 & -4 & -16N + \frac{\delta\omega C_t}{G_o} \end{bmatrix}$$

where $G_o = \frac{1}{R_o}$

$C_t = NC_s$ total electrode capacitance

N = transducer length measured in interdigital periods

(in other words: number of finger-pairs)

δ = a small increment in the transit angle θ

At synchronism, $\theta = 2\pi \frac{\omega}{\omega_o} = 2\pi$ and Y_{ij} becomes infinity. By setting $\theta = 2\pi + \delta$ and expanding to the first order of δ, Y_{ij} remains finite in the vicinity of ω_o.

An important feature of a transducer is the electrical immittance (impedance or admittance) it presents to its electrical port. This is composed of two elements: total electrode capacitance in combination with a radiation immittance representing acoustic wave excitation. The combination is either series or parallel, as illustrated in Fig. 29. It is assumed that there is negligible dissipation loss in the electrodes and that the acoustic ports are terminated with the characteristic impedance of R_o.

The immittance may be calculated for the "in-line" and "cross-field" models from the matrix expressions for $[Y]$:

in-line model: $$Z_3(\omega_o) = \left.\frac{E_3}{I_3}\right|_{\omega_o} = \hat{R}_a + \frac{1}{j\omega_o C_t}$$

where $$\hat{R}_a = R_a(\omega_o) = \frac{4}{\pi} k^2 \frac{1}{\omega_o C_s}$$

cross-field model: $$Y_3(\omega_o) = \left.\frac{I_3}{E_3}\right|_{\omega_o} = \hat{G}_a + j\omega_o C_t$$

where $$\hat{G}_a = G_a(\omega_o) = \frac{4}{\pi} k^2 (\omega_o C_s) N^2$$

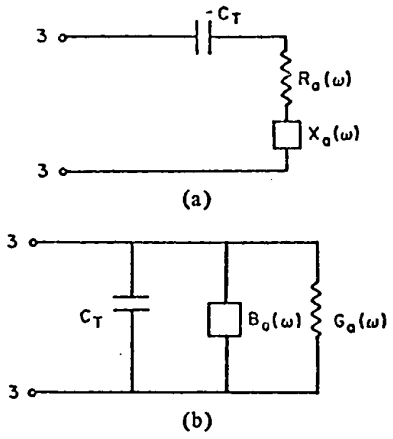

Fig. 29 Series and parallel representations of the array

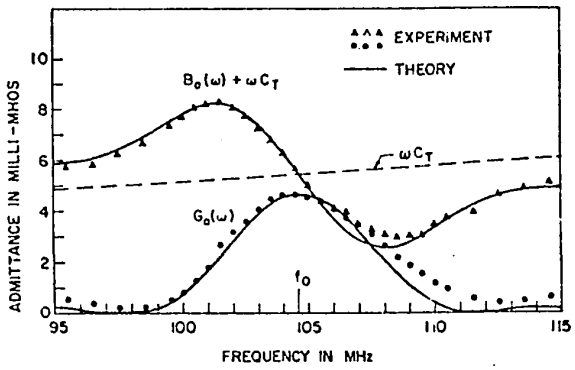

Fig. 30 Transducer admittance as a function of frequency

These forms indicate that the series representation (Fig. 29(a)) is suitable for the in-line model, whereas the parallel one (Fig.29(b)) suits the cross-field model. The reactive part (X_a or B_a) of the immittances vanishes in both cases at the resonant frequency.

In the weak coupling case ($\left[(4/\pi)k^2N\right]^2 \ll 1$) the input impedances of the two models are approximately the same. However, in the case of the more strongly piezoelectric cystals, such as lithium niobate, the difference is significant and an actual measurement of the impedance will indicate which is the appropriate model to use.

To examine the manner in which the immittances vary with frequencies away from ω_o, one has to go back to the general expressions, given by W.R. Smith et al [39]. The end results are stated here for frequencies near synchronism, for the crossed-field model (no equivalent expression is available in closed form for the in-line model):

$$G_a(\omega) \cong \hat{G}_a \left(\frac{\sin x}{x}\right)^2 \qquad B_a(\omega) \cong \hat{G}_a \frac{\sin 2x - 2x}{2x^2}$$

$$\text{where } x = N\pi \frac{\omega - \omega_o}{\omega_o} \quad \text{and} \quad \hat{G}_a = \frac{4}{\pi} k^2 \omega_o C_s N^2$$

These approximate expressions are accurate to within 10% provided $\omega - \omega_o/\omega_o < 0.2$.

Fig. 30 illustrates these relationships for the particular

case of YZ lithium niobate (Y-cut, Z-propagating) with N = 15. Experimental results confirm the curves to within 10%, lending support to the choice of a crossed-field model for this particular cut of lithium niobate.

Scattering and transmission characteristics of the transducer may also be evaluated from the matrix expressions for Y. A circuit of practical importance is one in Fig. 31(a), which will help to introduce the scattering coefficients. Here acoustic power is received at port 1, and depending on the nature of the electrical load Z_L, a certain amount of that power will be delivered to the load; part of it will be reflected back towards the generator and still another part will pass through and be delivered to the acoustic load at port 2.

A set of scattering coefficients p_{11}, p_{21}, p_{31} may be defined, where

$$p_{ij} = \frac{P_i}{(P_{avail})_j}$$

$L_{11} = -10 \log p_{11}$ = return loss at port 1

$L_{21} = -10 \log p_{21}$ = transmission loss from port 1 to port 2 through the transducer

$L_{31} = -10 \log p_{31}$ = transmission loss from port 1 to port 3, the electrical port

The values of these coefficients depend on the terminating conditions. For example, if Z_L is purely reactive,

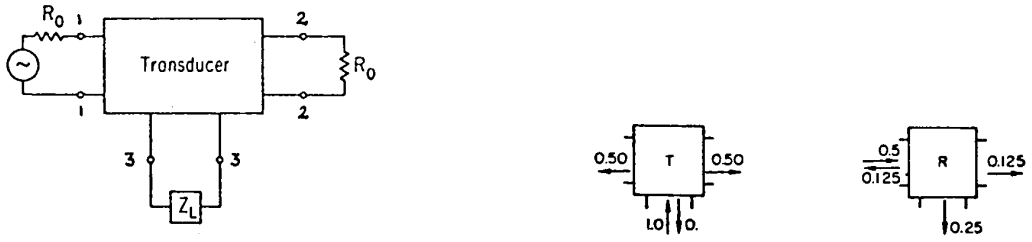

(a) (b)

Fig. 31 Transducer with matched acoustic terminations

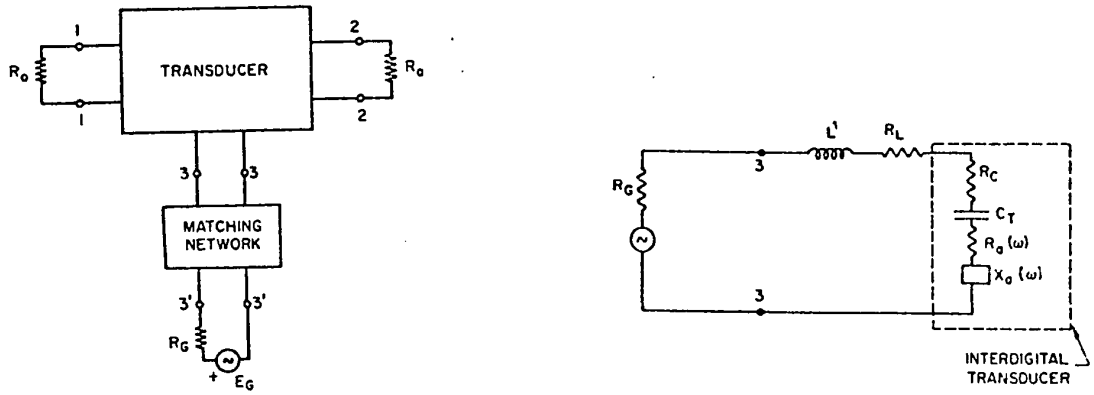

(a) (b)

Fig. 32 Schematic of a transducer with a matching network

$$p_{11} = \frac{1}{1 + a^2} \; ; \qquad p_{21} = \frac{a^2}{1 + a^2} \; ; \qquad p_{31} = 0 \; ;$$

$$\text{where} \quad a = \begin{cases} \dfrac{X_L - \dfrac{1}{\omega_o C_t}}{\hat{R}_a} & \text{"in-line"} \\[2ex] \dfrac{B_L + \omega_o C_t}{\hat{G}_a} & \text{"crossed-field"} \end{cases}$$

resulting in $L_{11} = 0$, $L_{21} = \infty$, $L_{31} = \infty$, in other words, complete reflection at port 1.

As another example, Z_L is to have a resistive component, i.e.:

$$Z_L = R_L + {}_j X_L \quad \text{with } X_L = \frac{1}{\omega_o C_t} \qquad \text{"in line"}$$

$$\text{or} \quad Y_L = G_L + {}_j B_L \quad \text{with } B_L = -\omega_o C_t \qquad \text{"cross-field"}$$

the resulting expressions for the p-coefficients are:

$$p_{11} = \frac{1}{(1 + b)^2} \; ; \qquad p_{21} = \frac{b^2}{(1 + b)^2} \; ; \qquad p_{31} = \frac{2b}{(1 + b)^2} \; ;$$

$$\text{where} \quad b = \begin{cases} \dfrac{R_L}{\hat{R}_a} & \text{"in-line"} \\[2ex] \dfrac{G_L}{\hat{G}_a} & \text{"cross-field"} \end{cases}$$

which leads to L_{11} = 6 db, L_{21} = 6db, L_{31} = 3 db for the case of minimum conversion loss (L_{31}). This requires a conjugate matched load (a = 0, b = 1) as evident from network theory too. Fig. 31(b) illustrates the relative quantities of power for a delay line with matched terminations.

The approach used in this analysis is also applied to a transducer of more complicated design by W.R. Smith et al [41]. Expressions are developed for input and scattering characteristics as well as design relationships for a dispersive interdigital transducer with non-uniform electrode spacing and non-uniform electrode length, as described in Section 3.5.

3.4 Transducer design principles

This section presents various design aspects and possible tradeoffs between characteristics of simple, nondispersive interdigital transducers. It is based on the work of W.R. Smith et al [40], utilizing the equivalent circuit model of Section 3.3. The design methods are aimed at achieving low insertion loss, broad bandwidth, high triple transit suppression and low phase dispersion. Since some of these pose conflicting requirements, compromises are necessary.

The electrical input impedance of the transducer can be represented as in Fig. 32(b) when the matching network is a simple tuning inductor (this series circuit corresponds to the "in-line" model of Section 3.3). $R_a(\omega)$ and $X_a(\omega)$ represent the frequency-

dependent resistive and reactive components of the acoustic radiation impedance, C_t is the total transducer capacitance, R_c stands for conduction losses in the transducer, L' is the tuning inductor and R_L denotes inductor losses. The acoustic ports in Fig. 32(a) are characteristically terminated. The circuit elements defining the transducer itself can be determined as follows:

a/ resistance R_c is a parallel combination of N individual fingers whose resistance can, in turn, be determined in the knowledge of its dimensions and material

b/ C_t is the sum of the individual interelectrode capacitances: $C_t = NC_s$, where C_s is proportional to w/L (w is the length of the electrode finger, L is the transducer period)

c/ the radiation impedance at synchronism is purely resistive ($X_a(\omega_o) = \hat{X}_a = 0$) and was determined by W.R. Smith et al [39] for the in-line model; it applies to the cross-field model as well.[1]

$$R_a = R_a(\omega_o) = (4/\pi)k^2 \frac{1}{\omega_o C_s}$$

---

[1] for the "cross-field" model:

$$\hat{Z}_a(\omega) = \frac{1}{\hat{Y}_a(\omega)} = \frac{1}{\hat{G}_a + j\omega C_t} = \frac{\hat{G}_a - j\omega_o C_t}{\hat{G}_a^2 + \omega_o^2 C_t^2} = \frac{(4/\pi)k^2\omega_o C_s N^2 - j\omega_o C_s N}{(4/\pi)^2 k^4 \omega_o^2 C_s^2 N^4 + \omega_o^2 C_s^2 N^2}$$

$$= \frac{(4/\pi)k^2}{\omega_o C_s (1 + 4/\pi\, k^4 \omega_o C_s N^2)} - j \frac{1}{\omega_o C_s N (1 + 4/\pi\, k^4 \omega_o C_s N^3)} =$$

For a given substrate material, k^2 is known, being a material property. A frequently used crystal is YZ $LINbO_3$ with a $k^2 = 0.05$, one of the highest couplings available. As mentioned in Section 3.3, the crossed-field model is the appropriate one for this example. From the expression for R_a, it appears that the factor available to manipulate the value of this conductance is C_s, i.e. w and L (see b/ above). At a given operating frequency, L is fixed, being equal to v/f_o (v is also a material property, fixed for a given crystal cut), leaving w (electrode length) as a means of varying the conductance. The reason for controlling transducer input impedance is the effort to create matching between transducer and generator (or load), a condition favoring high efficiency, i.e. low insertion loss.

$$\tilde{=} 4/\pi\, k^2 \frac{1}{\omega_o C_s} - j \frac{1}{\omega_o C_t}$$

which equals $\hat{Z}_a(\omega_o)$ for the "in-line" model, provided

$$(4/\pi) k^4 \omega_o C_s N^3 \ll 1$$

For YZ-cut $LiNbO_3$ transducer at 100 MHz, N = 5, $k^2 = 0.05$ and $C_t = 0.64$ pF,

$$(4/\pi) k^4 \omega_o C_s N^2 = (4/\pi) \times 25 \times 10^{-4} \times 2 \times 10^{8} \times 0.64 \times 10^{-12} \times 25$$

$$\tilde{=} 2 \times 10^{-5} \ll 1$$

Maximum efficiency is reached when source resistance equals transducer resistance, and the network (in a simple case, a tuning inductor) tunes out the static capacitance of the transducer. If resistive losses in the network (R_L) and the transducer (R_c) are negligible, efficiency approaches unity.

At frequencies other than resonance, the acoustic impedance becomes complex, due to the non-zero nature of $X_a(\omega)$, and the value of $R_a(\omega)$ or $G_a(\omega)$ changes. Mathematically:

"in-line"

$$R_a(\omega) \cong \hat{R}_a \left(\frac{\sin x}{x}\right)^2; \qquad X_a(\omega) \cong \hat{R}_a \frac{\sin 2x - 2x}{2x^2};$$

"cross-field":

$$G_a(\omega) \cong \hat{G}_a \left(\frac{\sin x}{x}\right)^2; \qquad B_a(\omega) \cong \hat{G}_a \frac{\sin 2x - 2x}{2x^2};$$

where $x = N\pi(\omega - \omega_o)/\omega_o = N\pi\delta$

Since acoustic power is connected with acoustic resistance or conductance, such a decrease in these latter quantities will reduce the generated power and limit the bandwidth of the device. This bandwidth, called the acoustic bandwidth, is conveniently expressed in terms of fractional bandwidth. On the basis of the above expressions, the half-power fractional bandwidth turns out to be:

$$B_a \cong \frac{7}{8N} \cong \frac{1}{N}$$

In a manner analogous to antenna arrays, therefore, as N increases, the acoustic bandwidth decreases. One may introduce a Q-factor to characterize this behaviour, designated Q_a. Being inversely related to bandwidth, Q_a is proportional to N.

There is also another factor determining the overall bandwidth of the device, and that is the bandwidth of the electrical circuit used to excite the transducer. In terms of Fig. 32, if $R_g = \hat{R}_a$ and $\omega L' = (\omega C_t)^{-1}$ the transducer is well matched to the generator since in the vicinity of ω_o the acoustic susceptance is comparatively small. The so-called electrical bandwidth, again characterized in terms of a Q-factor, will be:

$$Q_e = \frac{\omega L'}{R_g} = \frac{1/\omega_o C_t}{\hat{R}_a} = \frac{1}{\omega_o N C_s (4/\pi) k^2 (1/\omega_o C_s)} = \frac{\pi}{4k^2 N}$$

and, unlike Q_a, inversely proportional to N. The overall bandwidth of the device is controlled by the smaller one. For large N's, the acoustic bandwidth is significant and in fact equal to the total bandwidth; for small N's, the electrical bandwidth becomes the overall bandwidth. Obviously, there is one particular value of N, where the two bandwidths, hence the two Q's are equal, resulting in maximum bandwidth:

$$Q_a = Q_e$$

$$\text{or} \quad N = \frac{\pi}{4k^2 N} \qquad \text{and} \qquad N_{opt} = \sqrt{\frac{\pi}{4k^2}}$$

as it turns out, N_{opt} depends purely on substrate characteristics.

The optimum fractional bandwidth

$$B_{opt} = \frac{1}{N_{opt}} = \sqrt{\frac{4k^2}{\pi}}$$

illustrating the need for materials with strong piezoelectric coupling. For the strongest coupling material available, lithium niobate, $k^2 \approx 0.05$ under optimum conditions. This leads to $N \cong \sqrt{5\pi} = 4$ and $B_{opt} \cong 0.25$.

Transducers have been constructed with varying numbers of interdigital periods in order to verify the predictions of this circuit model. A single inductor was used to tune out part of the transducer reactance, i.e. the part due to interelectrode capacitance. The substrate was lithium niobate. Measured conversion losses vs. frequency were recorded with N as parameter, as illustrated in Fig. 33. The results bear out predictions to an excellent degree, showing the largest fractional bandwidth of 0.23 (between the 1.5 db points, corresponding to 3 db loss for the combined transmitter and receiver) at N = 5, which is closest to the number predicted by the model.

Another important aspect of transducer operation is the variation of phase-delay between acoustic and electric ports as a function of frequency, in other words, phase dispersion.

Constant delay or zero dispersion requires that total reactance remain approximately zero across the bandwidth. Fig. 30 shows the variation of acoustic reactance, which may be expressed as

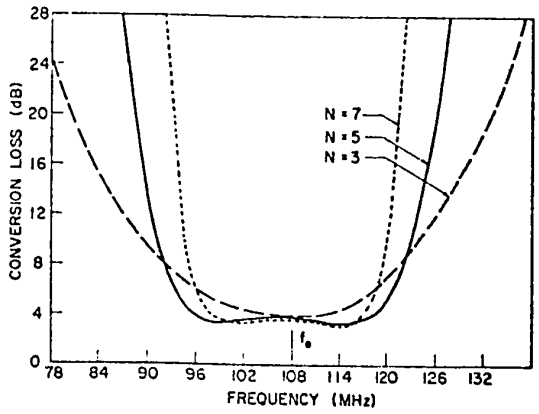

Fig. 33 Conversion loss of transducer with 3,5, and 7 periods

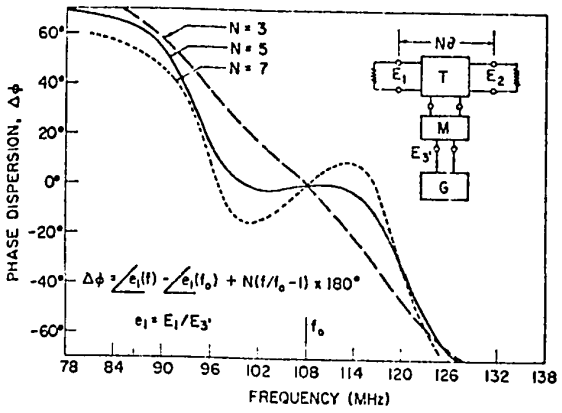

Fig. 34 Phase dispersion of transducer with 3,5, and 7 periods

$$X_a \cong -\frac{2\pi N}{3}\,\hat{R}_a\,\frac{\omega-\omega_o}{\omega_o}$$

The electrical reactance, due to the tuning inductance and the interelectrode capacitance (L' and C_t) can be written as:

$$X_e \cong \frac{2}{\omega_o N C_s}\,\frac{\omega-\omega_o}{\omega_o}$$

As seen in Fig. 32/b, these two are in series. To achieve $X = X_a + X_e = 0$ requires that

$$N^2 = \frac{3}{\omega_o C_s \hat{R}_a \pi} = \frac{3}{\pi}\,\frac{1}{k^2}$$

an almost identical expression to that obtained for maximum bandwidth. Fortunately, therefore, a transducer optimized for bandwidth will also be optimized for phase dispersion.

Measurements of phase characteristics were also made on the transducers of Fig. 33, and the results show excellent agreement once more with the predictions of the circuit model, as shown in Fig. 34. The curve corresponding to N = 5 (the number specified by the above equation for lithium niobate, $k^2 = 0.05$) displays the desired flatness to within 5^o over a bandwidth of 17 MHz. This band is 60% of the 1.5 db bandwidth for conversion loss in Fig. 33. The other two curves indicate the presence of obvious phase distortion.

Scattering parameters of transducers have also been predicted by the equivalent circuit model in Section 3.3 under speci-

fic terminating conditions. To verify predictions, a simple delay line was constructed, consisting of two transducers similar to the 5-period model of Figs. 33 and 34, and a delay path of YZ lithium niobate. The insertion loss of the device is defined as

$$IL\ (db) = 2L'_{13} + L_a \qquad (L_a = \text{acoustic transmission loss})$$

The triple transit suppression is given by:

$$TTS\ (db) = 2(L_{11} + L_a)$$

The theoretical insertion loss for matching conditions is 6 db, neglecting loss due to R_L and R_c as well as L_a, since at the frequency of operation (107 MHz) it is expected to be negligible. The theoretical TTS should be 12 db, as stated in Section 3.3, again neglecting transmission losses.

Experimental results again provided very good agreement with theory, both in magnitude and frequency dependence, with the exception of unexpected acoustic transmission loss, attributable to beam steering, i.e. diversion of the acoustic beam from its intended path due to faulty alignment of the transducer with the chosen crystalline direction.

Tradeoffs between some of these characteristics are available according to the circuit analysis of Section 3.3. One possibility is gaining improved triple transit suppression by creating a mismatch between radiation resistance of the transducer and source (or load) resistance. This can be achieved by manipula-

ting N or w. The consequence is either increased insertion loss (although the increase is less than that of the TTS), or decreased bandwidth or both.

One other tradeoff which may be attractive offers increased bandwidth at the expense of a slight increase of insertion loss. In involves a more elaborate matching network such as that of Fig. 35. With a transducer of N = 3, $\hat{R}_a = 135\,\Omega$, $C_t = 1.9$pF and $f_o = 108$ MHz on lithium niobate, the 3 db bandwidth of a delay line employing two such transducers and networks is 0.38. The matching network partially removes the cause of increased insertion loss at frequencies remote from synchronism: unmatched acoustic reactance. The network is designed to tune out that reactance over a fairly wide bandwidth; a slight overall increase in insertion loss is due to losses within the enlarged matching network

Other methods are also available to achieve increased TTS or bandwidth. One of these was already mentioned in Section 2.4, where acoustic amplifiers were introduced as an effective way of increasing triple transit suppression. Unidirectional transducers, discussed in Section 3.5 achieve similar results. In the same section, transducers with graded periodicity will be treated, whose features include large fractional bandwidths.

3.5 Variations of the basic array

In this section a description is presented of several transducer models that can be regarded as derivatives of the basic array

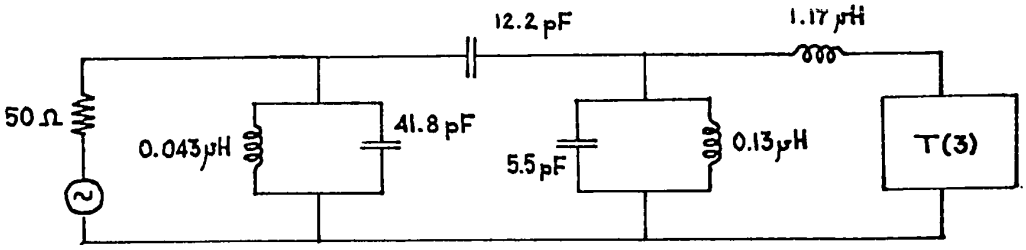

Fig. 35 Matching network for increased bandwidth

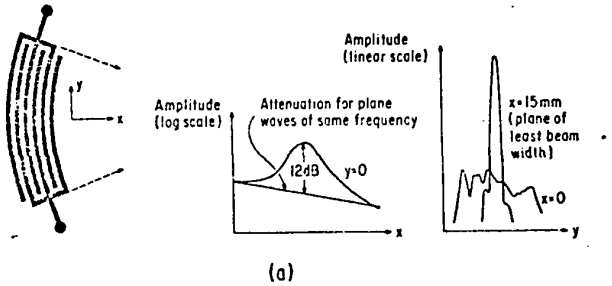

Fig. 36 Focusing interdigital transducer

of Sections 3.3 and 3.4. They are grouped into two categories:

1. Transducer types for the purpose of directing acoustic energy into a specific direction or region. This group includes unidirectional and focusing transducer arrangements.
2. Transducers with particular time, or frequency responses for filtering and other signal processing applications. Included here are arrays with variable electrode spacing, variable electrode overlap, and coded arrays.

Focusing transducers

Focusing arrangements through the use of acoustic lenses was mentioned in Section 2.4. Focused sources and receivers can also be constructed by properly shaping the elements of the transducer strip array. The acoustic wave emerging from the transducer electrodes is assumed to propagate in a direction perpendicular to the electrode. If the transducer has straight electrodes, a plane waveform is generated (neglecting diffraction due to the finite length of the electrode). By shaping the electrodes into segments of a circle as in Fig. 36(a), acoustic energy can be concentrated into a small area in the focus or center of the device. Fig. 36(b) shows measured variations of acoustic field strength along the x and y axes, and illustrating the focusing effect of the transducer. The substrate is transversely isotropic in order to avoid wavefront distortion [50].

Focusing of acoustic beams can also be achieved through the use of multistrip couplers, described by Marshall et al [28]. As illustrated in Fig. 37(a), they consist of a parallel combination of metallic strips across the acoustic path. It has been observed that transfer of acoustic energy takes place from track A (with an acoustic signal) to track B (with no acoustic signal in it originally). The transfer is due to currents induced in the strips, and becomes complete if the width of the coupler reaches a certain value L_T defined as the "transfer length". Fig. 37(a) shows an intermediate situation too, that of a half-transfer, occurring when the strip width is $L_T/2$. In this case, both tracks carry the same acoustic signal with the exception of a $\pi/2$ phase difference (adding another strip of width $L_T/2$ completes the transfer). This phenomenon led to the focusing strip of Fig. 37(b). The signals A and B in this case are parts of the same broad signal wavefront. Advancing the lower part of the strip by $\lambda/4$, the signal portion in track B is given the necessary $\pi/2$ advance, duplicating the conditions in the right hand side of Fig. 37(a). The emerging signal is now concentrated in track B, amounting to a narrowing of the beam, that is to say, focusing.

Unidirectional transducers

The basic array of the previous sections suffers from comparatively high insertion loss and low triple transit suppression, due to its bi-directional nature. They radiate equally in both forward and backward directions. Power in the backward direction

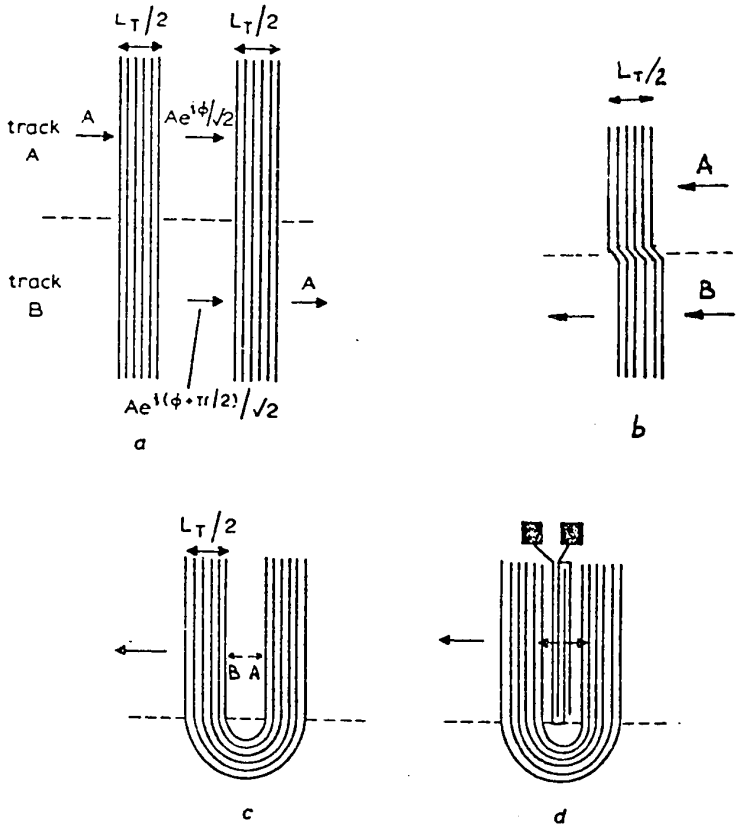

Fig. 37 Focusing by multistrip couplers

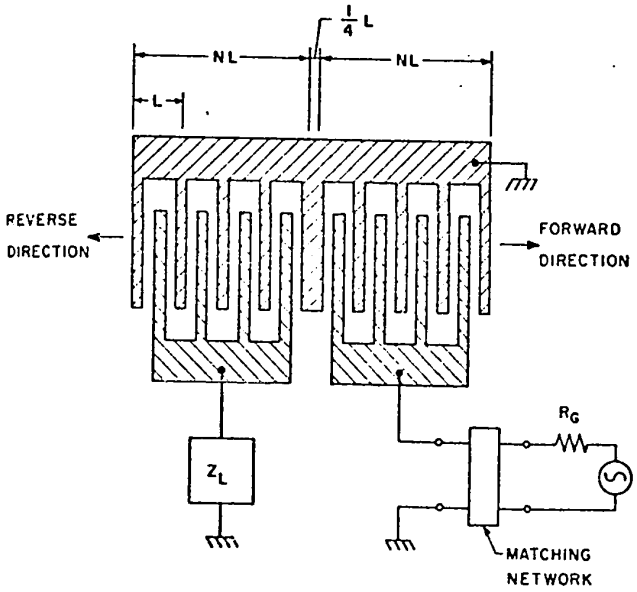

Fig. 38 Unidirectional transducer

is lost from the point of view of the receiver, resulting in a minimum of 3 db insertion loss for the transducer, or 6 db for a device including two transducers as transmitter and receiver (see Fig. 31(b)). The same mechanism gives rise to reflections in the receiving transducer, degrading TTS.

Several arrangements have been proposed to make transducers unidirectional. One scheme involves two identical arrays separated by a distance of $(n + 1/4)\lambda$ where λ is the surface wavelength, n is any integer. The arrays are driven with identical inputs but 90° apart, either from two separate generators, or a single generator with a $\lambda/4$ long transmission line connecting the two arrays [50].

A similar arrangement, illustrated in Fig. 38, involves the principle of parasitic reflectors for directive antennas. The same two arrays, $(n + 1/4)\lambda$ apart are employed, but only one of them is driven directly [40]. The second array is terminated with an inductor. This being a non-absorbing termination, all incident power is reflected, as mentioned in Section 3.3. In terms of that discussion, the reflection loss ratio p_{11} of the parasitic half of the transducer is:

$$p_{11} = \frac{1}{1+a^2} \qquad \text{where } a = \frac{B_L + \omega_o C_t}{\hat{R}_a} \quad \text{("cross-field" model)}$$

p_{11} becomes unity (i.e. a case of complete reflection) when $a = 0$. That happens when $B_L = -\omega_o C_t$, implying a negative load susceptance,

in other words, a pure inductance. What happens physically is analogous to the action of parasitic reflector antenna arrays: an acoustic signal is radiated by the driven transducer in both directions. One-half of the part radiating to the left will be received by the parasitic transducer, the other half will proceed through the transducer towards the left. The inductive load of the parasitic array reflects all of the received signal which will be reconverted into an acoustic signal with a 180° phase shift relative to the passing signal under the transducer. There will thus be cancellation towards the left. The reflected signal moving towards the right will rejoin the original right-traveling signal of the driven transducer in phase, due to the 180° phase-shift mentioned above plus twice the 90° (towards the parasitic transducer and back) due to the $\lambda/4$ separation of the two arrays.

Theoretically, zero insertion loss and infinite TTS could result in a delay line employing two such transducers. While actual performance is more modest, it still represents improvement over bi-directional transducers. Unfortunately, the design of Fig. 38 has inherently narrow bandwidth (about 2%) because as the frequency changes from resonance, load reactance no longer equals transducer capacitance and reflection is no longer complete from the parasitic array. A further reduction in bandwidth occurs due to having effectively doubled N, the number of finger-pairs in the complete transducer. To overcome this deficiency, the device of Fig. 39 has been proposed [18]. It places three

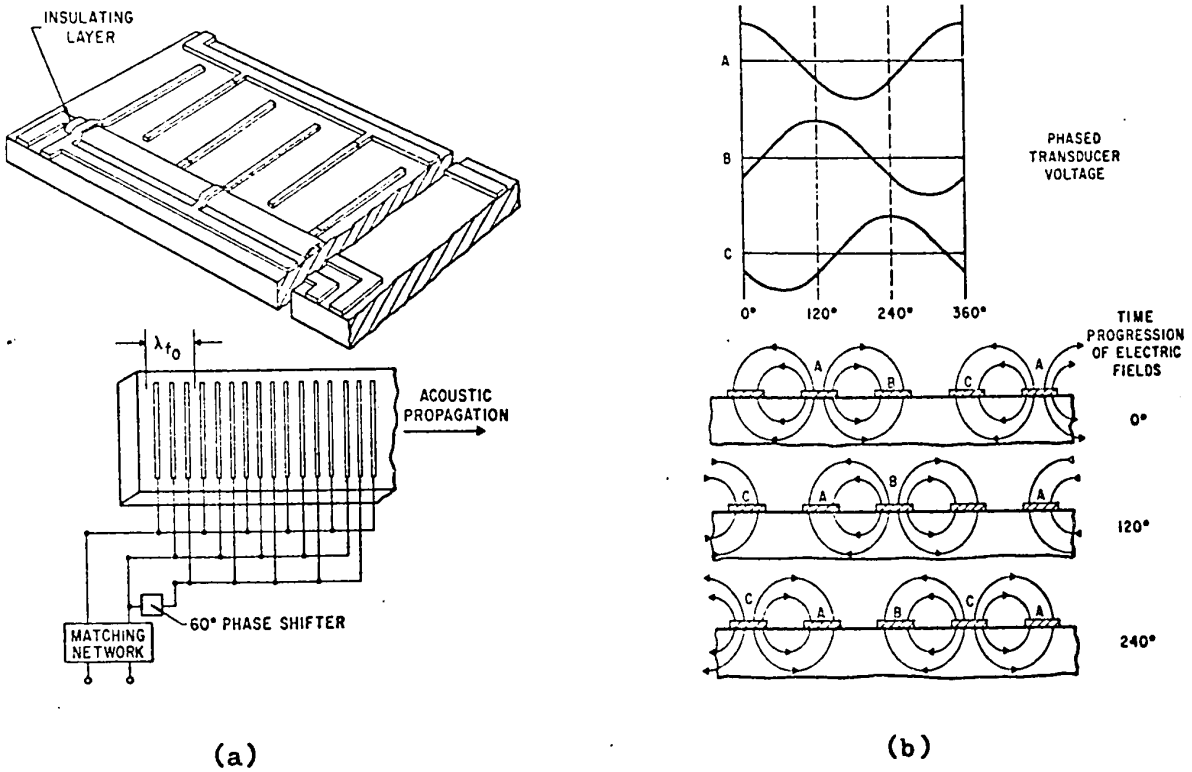

Fig. 39 Three-phase unidirectional transducer

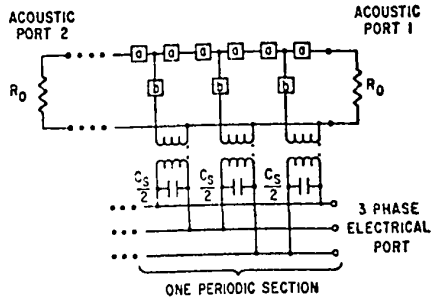

$R_0 = \frac{2\pi}{\omega_0 C_S k^2}$ $\qquad a = jR_0 \tan \theta/6$

$\theta = \frac{2\pi f}{f_0}$ $\qquad b = -jR_0 \csc \theta/3$

$C_{TOTAL\ PER\ SECTION} = \frac{3}{2} C_S$

C_S = CAPACITANCE PER SECTION FOR A BI-PHASE TRANSDUCER

k^2 = ELECTROMECHANICAL COUPLING CONSTANT

ω_0 = SYNCHRONISM FREQUENCY

Fig. 40 Equivalent circuit of three-phase array

sets of finger-like electrodes together in an interdigital fashion. The minimum of three sets of electrodes are required in any scheme in order to produce two independent fields necessary for one-directional operation. In the model of Fig. 38, the third set is the grounded array. In Fig. 39, all three sets are driven from the same source and a phase shifter provides a mutual phase difference of 120° between each array. Fig. 39 illustrates the electric field at three successive instants. The movement towards the right is evident, demonstrating the uni-directionality of the device [18]. Actual transducers constructed in this fashion yielded 20 db front-to-back ratio over a 20% bandwidth on YZ $LiNbO_3$ at 10.7 MHz.

Analysis of the transducer of Fig. 39 can be performed in the same manner as that of the basic array, based on the equivalent circuit, appropriately modified as in Fig. 40.

Still another unidirectional transducer design follows from the multistrip coupler applications of F.G. Marshall et al [28] introduced under "focusing transducers" and illustrated in Fig. 37. Using Fig. 37(b) as a starting point, it is apparent, that similar results can be achieved if the strips are straight and the two signals arrive in phase quadrature instead (as in Fig. 37(a)). Furthermore, it is not necessary to visualize the two signals as travelling parallel with each other and in the same direction. For example, if the strip is now formed into a U-shape as in Fig. 37(c), an operation which will not affect the behaviour of the strip

since currents in it continue to flow as before, and two signals of equal amplitude and in phase quadrature are impressed on the two sections, a signal will only emerge from one of the sections. The two signals in question can be conveniently generated by an ordinary bidirectional transducer placed inside the U-shaped strip, offset from the center by $\lambda/8$. This will produce the required $\pi/4$ phase-difference between signals A and B and the result is a unidirectional device, as shown in Fig. 37(d). This is also a broad-band transducer, with the added advantage of not requiring external components for phase shifting. The reflector strips are deposited on the substrate in the same fabrication process as the transducer in the centre.

Transducers with non-uniform geometry

This class of transducers may be arranged into two groups:

(a) transducers whose frequencey response is modified by varying the finger spacing, overlap or both (chirped transducers)

(b) coded transducers with uniform spacing and overlap, but with electrodes connected to the source in a specifically coded sequence

Chirped transducers

Arrays of the first group are more sophisticated versions of the basic array, taking advantage of the opportunity of manipulating the transducer response by allowing either the electrode

spacing or electrode overlap, sometimes both, to vary as illustrated in Fig. 41(a), (b), and (c) respectively.

An example of the use of non-uniform array is a delay line with a relatively broad-band response. One way of achieving a large fractional bandwidth was mentioned in Section 3.4 involving an elaborate external matching network. Such a network is often cumbersome in microcircuit fabrication. Instead, broad-banding is achieved through the use of graded periodicity, as in Fig. 41(a). Each section of the transducer is resonant to a different frequency and may be thought to have an individual frequency response determined by the number of fingers of approximately correct spacing. The overall bandshape is the sum of the individual overlapping responses, hence it may be made fairly wide. Delay lines may be non-dispersive or dispersive, the latter type having applications in the field of amplitude, or phase equalization.

Another important field of application involving special transducer arrays is that of acoustic filters. These can be synthesized from their specified time or frequency responses by properly selecting the necessary transducer geometry. These filters may be the usual band-pass variety such as IF filters for television receivers, or matched filters with specified time response as required in radar circuits.

The characteristics of the transducer of Fig. 41(c) (which account for those of (a) and (b) as well) have been evaluated by

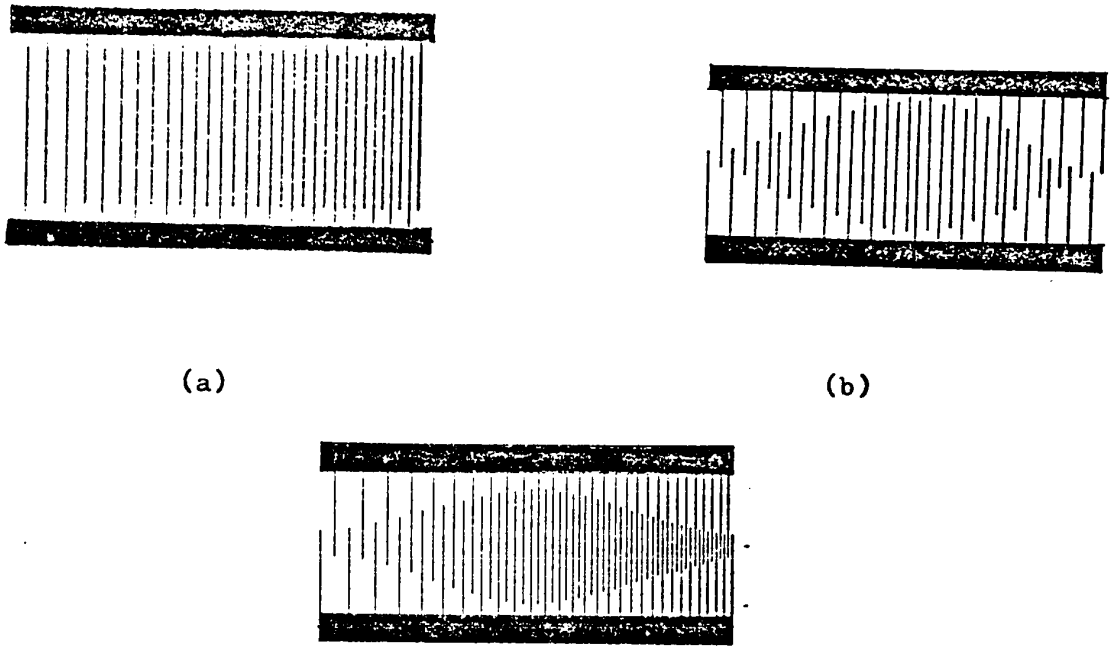

(a) (b)

(c)

Fig. 41 Transducers with non-uniform spacing and overlap

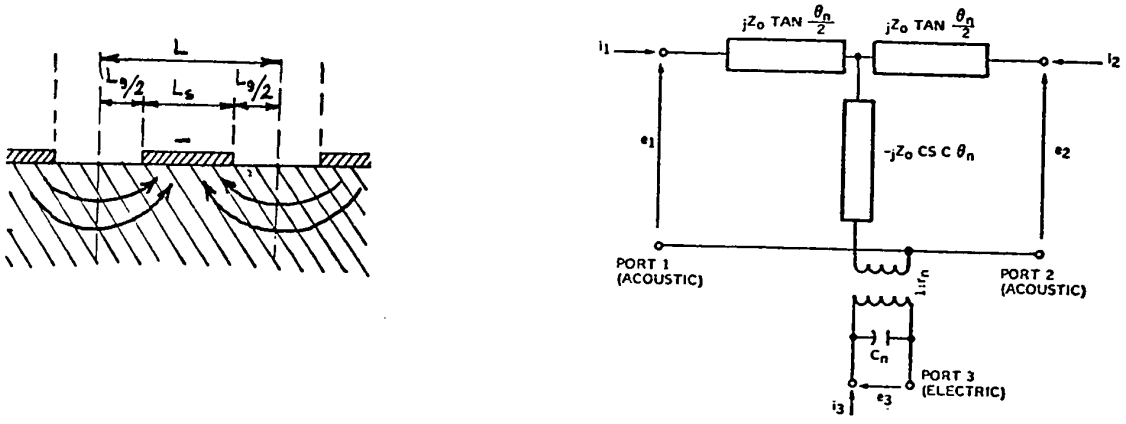

(a) (b)

Fig. 42 Equivalent circuit for non-uniform transducer

W.R. Smith et al [41]. Their analysis is based on an extension of the model in Section 3.3, redrawn slightly in Fig. 42 to a form more suitable for expansion. This particular circuit represents the "cross-field" model, one that is somewhat more simple mathematically than the "in-line" model (a choice must be made in a given case between the two models, depending on the substrate in question as discussed in Section 3.3). Since the electrode spacing is variable now, different values must be assigned to the circuit elements in Fig. 42(b) for each section.

$$\theta_n = \pi f / f_n \qquad \text{where} \quad f_n = v/2L_n$$

$$C_n = \frac{w_n\sqrt{\epsilon_{11}\epsilon_{33}}}{2}\frac{K(q_n)}{K(q'_n)}$$

where w_n = acoustic aperture (length of overlap)

$\epsilon_{11}, \epsilon_{22}$ = substrate dielectric tensor components

K = Jacobian complete elliptic integral of the first kind

$$q_n = \sin(\pi L_{s_n}/2L_n)$$

$$q'_n = \sqrt{(1 - q_n^2)}$$

$$r_n = (-1)^n\sqrt{2f_nC_nk^2Z_o}\,\frac{K(2^{-1/2})}{K(q_n)} \qquad \text{(transformer ratio)}$$

The transducer arrays discussed in this section often have a large number of electrodes, sometimes in the order of thousands. In section 3.3 reference was made to the necessity of

taking into account the acoustic impedance discontinuity caused by the metallic electrodes. The resulting reflections can combine into significant echoes when the transducer is large (large N) and when the substrate has strong piezoelectric coupling. This being frequently the case here, a better estimate of the device performance can be made by replacing the simple equivalent circuit of an electrode unit with the more elaborate one allowing for this effect, as shown in Fig. 27.

By making the aperture (w) a function of position (n), we introduce variable overlap or "apodization", as in Figs. 41(b) and 41(c). It has been observed that surface waves generated by apodized transducers of this type suffered from phase distortion. This was traced to the fact that as straight acoustic wavefronts traversed the transducers, the edges of the front encountered less electrode surface than the center part. Since the electrodes alter the phase velocity (as explained in Section 3.3), this situation gives rise to unequal phase changes in the wave. To correct this condition, phase-correcting "dummy" electrodes were added, as in Fig. 43. These added electrodes do not participate in the generation (or reception) of acoustic signals, since they do not face electrodes of different potential [17].

As in Section 3.3, Fig. 28, the equivalent circuits of Fig. 42 are interconnected in a cascading configuration to form the complete equivalent circuit of the transducer. In this case, the component blocks being different, it is not possible to develop

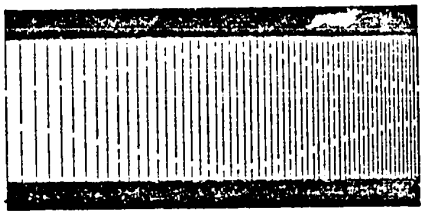

Fig. 43 Transducer with phase-compensating electrodes

a simple expression for the admittance coeffcients Y_{ij} of the complete transducer. They can be evaluated nevertheless, with the aid of computers.

The connection between the spatial characteristics (i.e. t_n: electrode position, w_n: aperture) of the transducer and its frequency or time response has been analyzed by W.R. Smith et al [41]. with the following design equations as final result:

$$\phi(t_n) + \tan^{-1} \frac{Q_L e(t_n)\phi(t_n)}{2\pi f_o e(t_n) + Q_L \dot{e}(t_n)} = n\pi \qquad n = 1,2,\ldots,N$$

N = number of finger-pairs

$$\text{and} \quad w_n = A(f_n/f_o)^{-3} \frac{K(q_n)K(q_n)}{\left[K(2^{-1/2})\right]^2} \left\{ \left[e(t_n) + \frac{Q_L}{2\pi f_o} e(t_n) \right]^2 + \left[\frac{Q_L}{2\pi f_o} e(t_n)\phi(t_n) \right]^2 \right\}$$

The explanation of the terms:

a/ f_o is a conveniently chosen reference frequency

b/ Q_L is the load Q, defined as $Q_L = 2\pi f_o C_t / G_L$

where G_L = load conductance

C_t = total transducer capacitance, equal to sum of C_n's

The load Q is controlled by the impedance ot the external electrical networks and by the acoustic aperture, since they determine C_t. Its value determines transducer efficiency through its scattering characteristics. When it is high, large amount of reflection takes place. When it is low, most of the surface wave power passes under the transducer undisturbed. When it

is about unity, efficiency is at maximum. Its actual value is chosen according to the design requirements. This combined with the fact that G_L is usually fixed, necessitates the presence of some adjustable constant in the design equation for w_n, in order to satisfy the defining equation for Q_L. This constant is A.

c/ K (q_n)'s are the Jacobian integrals mentioned previously in this section

d/ $\phi(t)$ and e(t) are the components of the externally specified time response of the transducer, more specifically, its impulse response, h(t)

$$h(t) = e(t) \exp\left[j \phi(t) \right]$$

Design specifications are conveniently expressed in terms of h(t), because a transducer is a device that takes time samples of a waveform [41]. When the transducer transfer function H(f) is given, it is necessary to calculate the associated time response h(t) which is the Fourier transform of H(f).

In delay line and filter applications where the complete device response, rather than individual response is specified, transducer transfer functions must be selected in such a way that their product equals the desired filter transfer function. In one type of device the two transducers are identical in terms of finger spacing and aperture distribution. There are two possible

orientations here: in the first, the two transducers are similarly oriented as in Fig. 44(a). This arrangement is nondispersive, as may be seen by the following argument: Any one particular frequency component of an applied signal will originate in a specific region of the transducer, where the spacing is synchronous with this frequency. In the receiving transducer there is a corresponding region which will respond to this frequency component. The distance between the two regions is a constant regardless of the frequency chosen, because of the identical geometry and orientation of the two transducers. All frequency components therefore travel the same distance and since the substrate itself is nondispersive, all are delayed equally. It is apparent that the device of Fig. 44(a) is basically a broad-band one, as it is capable of responding to a wide range of frequencies due to its "chirped" spacing.

The other possible orientation of the two transducers is illustrated in Fig. 44(b). It is a broad-band device, like the previous one, but has a dispersive frequency dependence. Another combination of transducers that may be employed to satisfy a specified overall transfer function consists of an array with only a small number of electrodes with constant spacing and overlap and a more complicated comb of the type just discussed [44]. The small array has a flat broad-band response to a first approximation, hence the detailed response H(f) is determined primarily by the "chirped" transducer.

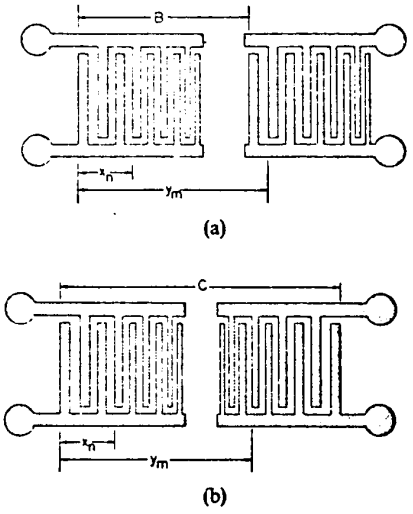

Fig. 44 Non-dispersive and dispersive filters

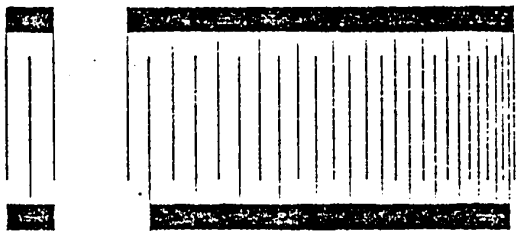

Fig. 45 Simple surface wave filter

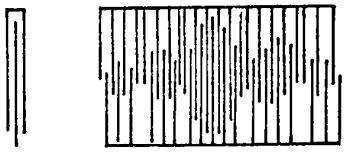

Fig. 46 Acoustic bandpass filter

Fig. 45 shows the basic arrangement; the right-hand transducer is shown as having constant overlap to illustrate the fact that some types of frequency responses can be realized by one variable (either spacing or aperture) only. In general however, both variables must be utilized in order to realize both amplitude and phase variations of the required response.

In the following, a few applications of these transducers are described. A typical device is a band-pass filter. It can be synthesized with a combination resembling that of Fig. 45, insofar as the burden of matching the required response falls on the receiving array. The response can be met by a uniformly spaced array with an aperture distribution equalling the Fourier transform of the desired frequency response, i. e. a sin x/x pattern, illustrated in Fig. 46 [44]. The necessary phase change at the nulls is achieved by a finger connection reversal.

Another application calling for similar arrays is the pulse compression filter used in radar and communications systems where the problem is target recognition in the presence of noise. When there are limitations regarding peak transmitter power, performance can be improved by employing signal formats with a large time-bandwidth product. This will improve receiver S/N at the expense of fewer target recognitions per second. A popular signal format is a linear frequency modulated or "chirped" signal of Fig. 47(a). When such a signal is delivered to the receiving transducer of Fig. 47(b), the finger spacing is arranged to coincide with

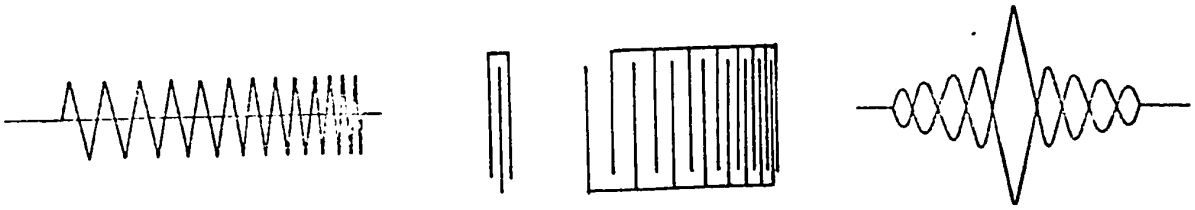

(a) (b) (c)

Fig. 47 Pulse compression filter

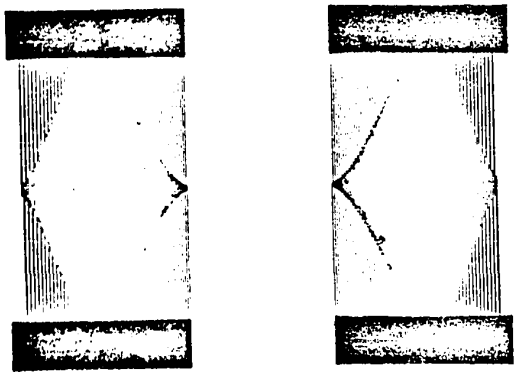

Fig. 48 Improved pulse compression filter

the signal pattern the moment it fills the receiver, all electrode pairs resonate simultaneously, producing the large lobe in the center of Fig. 47(c)[22]. A certain amount of sidelobe power is generated at times preceding and following the main lobe. They are the natural consequence of the sudden termination of the comb and can be reduced by a more sophisticated design involving a pair of apodized arrays as in Fig. 48, in a dispersive configuration [44]. Sidelobe power is considerably reduced at the cost of a slight increase in main lobe width. Pulse compression ratios of 100:1 can be achieved in this manner.

Coded transducers

Coded transducers are also employed in situations similar to the previously discussed one, where the compression of an RF pulse is implemented through the use of a "matched filter" [20].

Matched filters possess a response which is "matched" to the frequency, amplitude and phase of one particular kind of uncompressed waveform. The outputs from the filter elemets are synchronously additive only when the correct waveform is presented to the filter. To accomplish this, the impulse response of the matched filter must be a time-reversed copy of the uncompressed waveform.

Fig. 49 illustrated the principle of operation of the matched filter for a radar signal encoded by a phase-switched scheme. In this case, the encoded signal was one of constant amp-

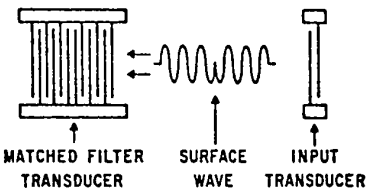

Fig. 49 Matched filter

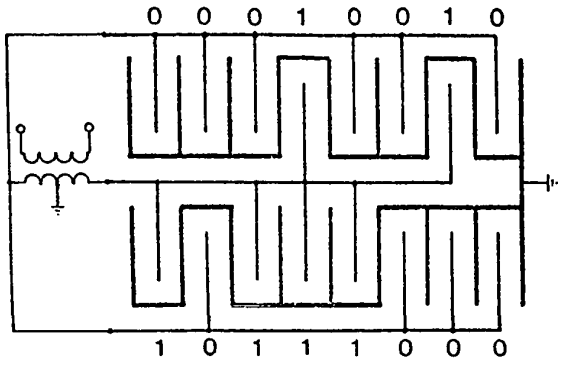

Fig. 50 Coded transducer

litude and frequency, with phase reversals in a certain pattern for which the receiver was constructed. At the instant the illustrated surface wave pattern is under the electrodes that properly coincide with the spatial distribution of the signal, a large output peak is generated. The size of the sidelobes, a critical matter, is determined by the coding scheme and the number of elements contained in the code. Certain code sequences have been designed to yield low-amplitude time sidelobes. One class of such codes is a set of so-called Barker codes. These have sidelobes which are at the most, 1/n of the correlation peak, where n is the number of elements in the code. In Fig. 49 for example, the 6-element code would produce an output pulse at least six times larger than the largest sidelobe.

Another set of codes, known as Golay codes exists in pairs of complementary series. The autocorrelation functions of these have sidelobes of equal magnitude and opposite sense. They can be summed resulting in theoretically complete cancellation of sidelobes, when these coded signals are propagated in parallel, complementary coded delay lines. An example of such an arrangement is shown in Fig. 50 [32]. The two separate lines with the common push-pull drive generate the two complementary codes 00010010 and 10111000.

These coding schemes allow surface area to be used efficiently [22], achieving wide bandwidths and good impedance match with source, by stretching the transducer out along the propagation

path.

The signals of Fig. 48 and Fig. 49 can be characterized as having a large time-bandwidth product. This has particular significance in matched filter applications where the purpose is to transmit signals in a time-expanded form and receive them through a pulse compression filter [38]. By selectively delaying various parts of the input signal to produce an approximate delta function at the input, the filter maximizes the signal-to-noise ratio:

$$(S/N)_{out} = \frac{\text{signal energy}}{\text{power spectral density of input noise}} =$$

$$= \frac{\text{mean signal energy}}{\text{mean input noise power}} \times TB$$

For given mean signal and noise powers, the S/N will increase if the time-bandwidth product of the signal is increased. This is achieved by encoding the signal into the frequency-sweep or phase-switched formats just described. Both formats involve a constant-amplitude signal, where mean signal energy is related to peak signal power by a simple constant factor. The usual limitation in typical applications, such as radar, is peak transmitter power, in this case also mean signal power. To achieve the required range and resolution (high S/N), the matched filter must have the necessary high TB product as well.

CHAPTER 4

SURFACE WAVE DEVICE FABRICATION

4.1 Material considerations

The preceding sections have outlined a large number of actual and potential applications for surface waves. The performance and success of these devices hinges to a large extent on the availability of a wide choice of suitable materials [50], [12].

A particularly wide assortment is required for the newly emerging type of devices utilizing layered construction, such as the various combinations of slow-on-fast and fast-on-slow wave-guiding structures, surface wave amplifiers with semiconducting films on piezoelectric insulators, piezoelectric films on isotropic substrates for transduction, among others. Even devices of a more simple construction like metallic transducers on bulk substrates may have varying material demands depending on the circumstances of application.

The most important material properties for use in the latter group are: electromechanical coupling factor, surface wave velocity and suitability for microelectronic fabrication. The first of these, (k), determines the maximum fractional operating bandwidth, compatible with minimum insertion loss, of delay lines, as stated in Section 3.4 for uniformly spaced interdigital transducers [13].

$$B_{opt} = \frac{1}{N_{opt}} = \sqrt{\frac{4}{\pi} k^2}$$

The surface wave velocity determines the information storage capability of a given length of delay line-or simply its delay. Also, through the relationship:

$$\text{transducer periodic spacing} = \frac{\text{acoustic velocity}}{\text{frequency}}$$

it has an effect on the maximum operating frequency of a transducer with a given electrode spacing.

Suitability for microelectronic fabrication is obviously related to cost and yield of manufacture. Table I summarizes the important characteristics of some of the more frequently used piezoelectric substrates, from the point of view of transducer design [40]. The quantity $\Delta v/v$ is approximately equal to $k^2/2$, as mentioned in Section 2.3, N_{opt} is the number of transducer periods required for optimum operation, M_{opt} is the aperture width in wavelengths which will yield a radiation resistance R_a of 50 ohms, assuming $N = N_{opt}$, $\Delta\omega/\omega_o$ is the maximum fractional bandwidth (referred to as B_{opt} before), T is the delay in μs/cm, i.e. the inverse of surface velocity, $T\Delta\omega/\omega_o$ is the time-bandwidth product. The table indicates that whereas lithium niobate has the largest fractional bandwidth due to its high coupling ($\Delta v/v$), bismuth germanium oxide has a larger TB product on account of its low velocity of propagation hence it appears to be more suitable for matched filter applications. On the other hand, where large bandwidths are required, lithium niobate tends to have the advantage.

TABLE I

OPTIMUM TRANSDUCER DESIGN FOR VARIOUS SUBSTRATES

Piezo-electric	Cut and Propagation Direction*	$\frac{\Delta v}{v}$ (%)	N_{opt}	M_{opt}	$\frac{\Delta\omega}{\omega_0}$	T (μs/cm)	$T\cdot\frac{\Delta\omega}{\omega_0}$
$LiNbO_3$[4]	YZ	2.46	4	108	0.24	2.88	0.69
$Bi_{12}GeO_{20}$[5]	[110], [$\bar{1}$10]	1.15	6	183	0.17	6.33	1.08
ZnO[5]	XZ	0.56	8	99	0.12	3.74	0.45
Quartz[6]	YX	0.11	19	53	0.053	3.06	0.16
PZT[7]	†	2.15	4	—	0.23	4.55	1.04
CdS[7]	XZ	0.31	12	54	0.09	5.82	0.52
$LiTaO_3$[7]	ZY	0.82	7	31	0.14	2.86	0.40

* The first symbol refers to crystal cut and the second to propagation direction; this notation will be used henceforth in the text.

† Poled normal to surface; propagation isotropic within the surface.

TABLE II

Materials	SURFACE WAVE VELOCITIES Cut	Velocity (10^5 cm/s)
Quartz	Y-cut, x-prop.	3.154
"	x-cut, y-prop.	3.26
"	z-cut, x-prop.	3.258
"	fused	3.42
CdS,	basal plane (piezoel. stiff.)	1.731
"	along C-axis (")	1.707
GaAs	normal (111) prop (110)	2.429
"	" (001) " (110)	2.863
"	" (110) " (110)	2.399
InSb	" (211) " (011)	1.674
"	" (211) " (111)	1.780
$LiNbO_3$	" (010) " (100)	3.858
"	" (001) " (100)	3.873

Extensive work has been done to investigate the properties of various substrate materials. As the majority of these is in a crystal form, the properties tend to vary according to the cut and direction of propagation relative to the crystalline axes. Table II. illustrates the variation of one significant parameter, surface-wave velocity [46].

The variation of the electromechanical coupling constant with crystalline direction is also an important aspect of piezo-electric material behaviour. Its knowledge helps to select the most favorable cut for a given application. Fig. 51 shows the results of measurements for $LiTaO_3$ in terms of $\Delta v/v$, for three different crystal cuts [34]. The other curve in these diagrams, designated: "power flow (deg.)", indicates the angular difference between time-average electromechanical power flow and phase velocity vector as a function of direction of propagation. As seen in the diagrams, the angular difference becomes zero (i.e. the two directions coincide) at the peaks of the $\Delta v/v$ curve. Similar graphs have been worked out for other materials, such as $LiNbO_3$ by Campbell and Jones [9], and $Bi_{12}GeO_{20}$ by Slobodnik and Budreau [35].

It should be noted that the quantity $\Delta v/v$ equals $1/2\ k^2$ only when the assumption of an infinitely thin conductive layer is satisfied. When this is not the case, the change in velocity will be partly due to the shorting of the electric field, and partly to the mechanical loading of the surface by the mass of the

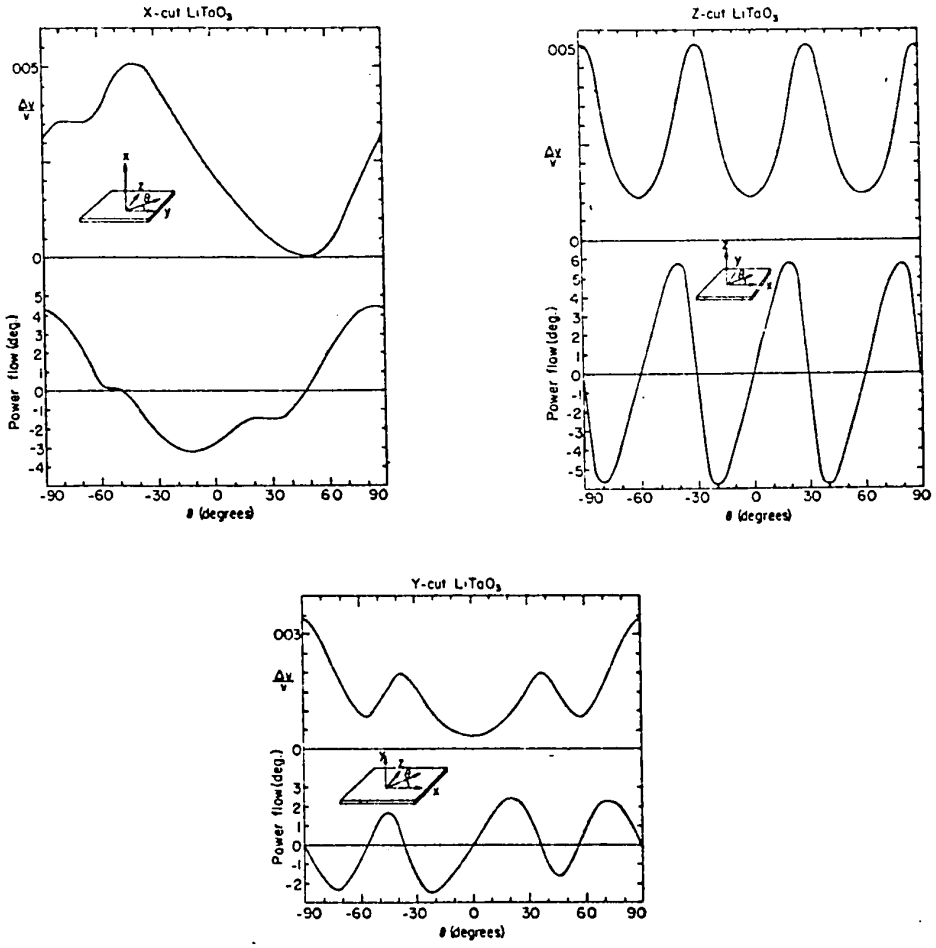

Fig. 51 Coupling and power flow vs. crystal orientation in $LiTaO_3$

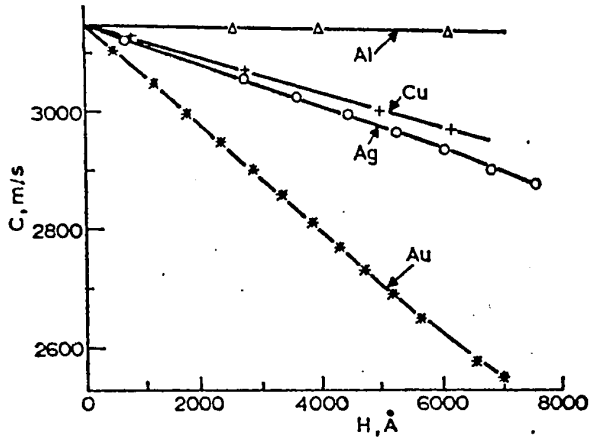

Fig. 52 Effect of electrode thickness on phase velocity

electrodes. In the extreme, when piezoelectricity is weak or non-existent, the velocity change is a result of mechanical loading only. Quate and Cambon [30] performed a series of measurements in order to determine the loading effect of various metals as a function of electrode thickness. The results appear in Fig. 52. The substrate used was quartz, which possesses very weak piezoelectric coupling. The diagrams indicate that aluminum electrodes place the least amount of loading on the surface, while gold represents the heaviest loading.

Another important characteristic of substrate materials is the variation of surface wave velocity with temperature. The significance of this is obvious in delay line or phase equalizer applications. As with many other characteristics, temperature coefficients were also observed to vary with crystalline direction. Fig. 53 shows the results of measurements for $LiTaO_3$ [34]. The lower set of readings corresponds to the temperature coefficient of delay, defined as

$$\frac{1}{\tau}\left[\frac{\partial \tau}{\partial T}\right] = -\frac{1}{f}\left[\frac{\partial f}{\partial T}\right]_{\phi}$$

where τ is the delay time, f is the frequency of the test-pulse, T is the temperature and ϕ is the phase. The temperature coefficient of velocity is a related quantity, defined as

$$\frac{1}{v}\frac{dv}{dT} = \alpha - \frac{1}{\tau}\left[\frac{\partial \tau}{\partial T}\right]_{\phi}$$

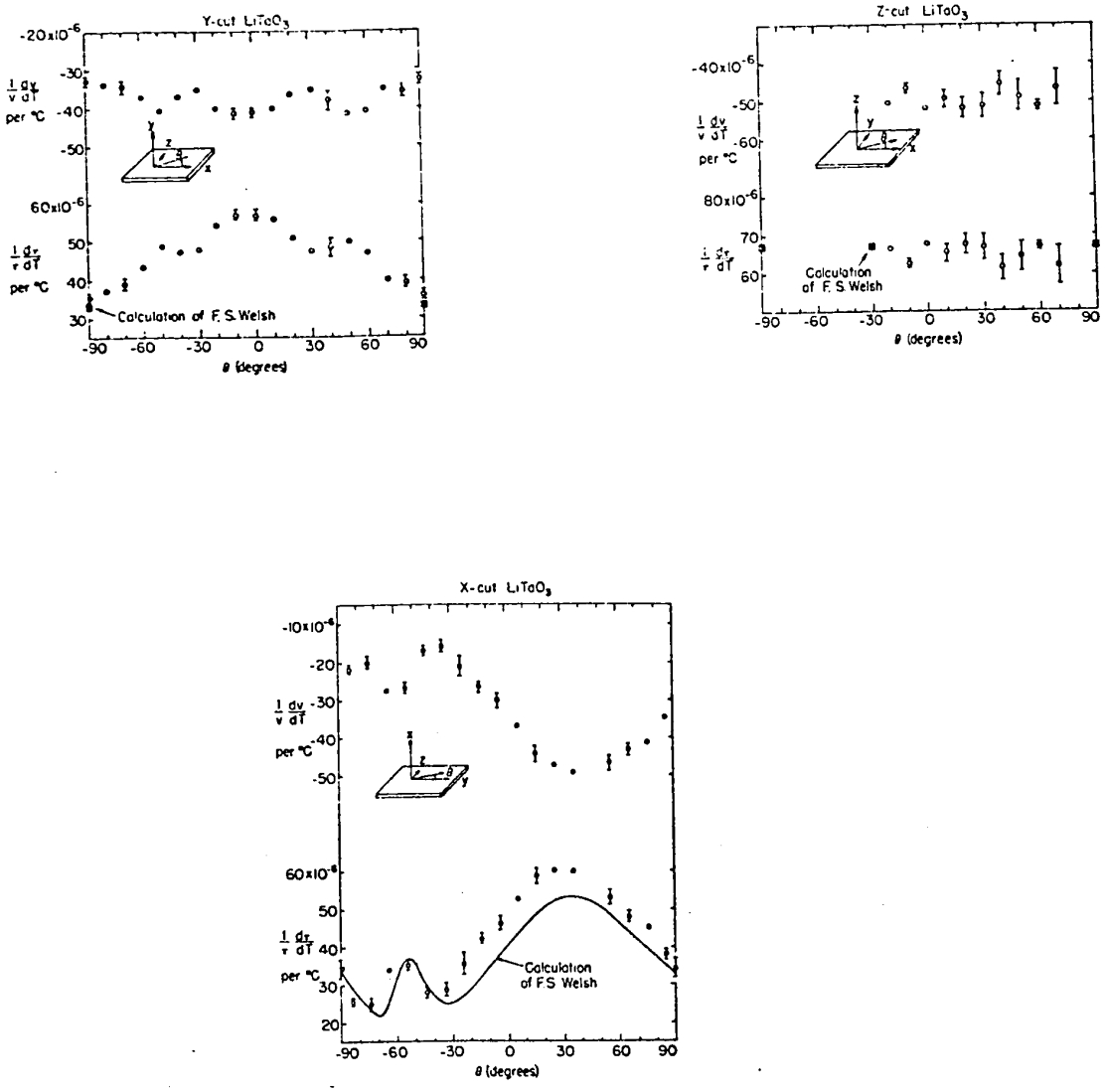

Fig. 53 Temperature coefficients of surface velocity in $LiTaO_3$

where v is the velocity of surface waves and α is the thermal expansion coefficient of the substrate. The upper set of readings of Fig. 53 indicate measured values of the temperature coefficient of velocity. The error bars appearing with the data points show the range of values obtained in different temperature ranges. Their presence indicates that second or higher order temperature coefficients exist. The solid lines serve as comparison with calculated coefficients, by F.S. Welsh [47].

While there is appreciable variation of temperature stability among various materials as well as cuts of the same material, no direction provides completely temperature-independent behaviour. When the naturally available performance is not sufficiently good, temperature controlled ovens, or external stabilizing circuits may be employed [49].

Other characteristics that may become significant are nonlinear elastic behaviour (for mixing and parametric applications), mechanical strength, hygroscopy, dielectric and chemical properties (solubility, compatibility with etchants and resists), uniformity in desired crystalline orientations, and not the least, cost.

The following is a brief review of the salient features of the most frequently used piezoelectric substrate materials. They may be grouped as single crystal types, compound semiconductor materials and ceramics. In the first group are found some

ferro-electric materials such as:

a/ lithium niobate ($LiNbO_3$)

b/ lithium tantalate ($LiTaO_3$)

c/ barium sodium niobate ($Ba_2NaNb_5O_{15}$)

as well as non-ferroelectric ones:

d/ crystalline quartz (SiO_2)

e/ bismuth germanium oxide ($Bi_{12}GeO_{20}$)

f/ lithium gallate ($LiGaO_2$)

g/ lithium iodate ($LiIO_3$)

among the compound semiconductor materials are:

h/ cadmium sulfide (CdS)

i/ zinc oxide (ZnO)

the most important among the ceramics is:

j/ lead titanate zirconate (PZT)

a/ Lithium niobate (rhombohedral, point group /3m/) has been widely used in surface wave applications, because of its high coupling and relatively low acoustic losses. Its disadvantages include high cost and manufacturing difficulties. The crystal is brittle and requires poling to achieve the low losses. Being such an important substrate material, lithium niobate has been the subject of extensive investigations. An example of this work is that reported by Slobodnik and Szabo [36]. The purpose of their investigations was to identify favorable crystalline directions in the material. Table III. summarizes the properties of the crystal in three particular directions. Each of these can offer certain favorable features such as low dif-

TABLE III

COMPARISON OF THE 16½° DOUBLE-ROTATED CUT OF $LiNbO_3$ WITH THE YZ- AND 41½°-ROTATED CUT ORIENTATIONS

	16½°-double-rotated cut	*Y* Cut *Z* Propagating	41½°-rotated cut
Surface-wave velocity, m/s ($\omega h = \infty$)	3503	3488	4000
$\Delta v/v_\infty$	0·0268	0·0241	0·0277
3 dB diffraction-loss time delay, μs	29·3	30·5	5·29
3 dB beam-steering-loss time delay, μs	16	14	37
Measured untuned delay-line minimum insertion loss, dB	23·6	26·45	17·71
Measured reflection losses due to transducer mismatch, dB	3·30	6·79	0·27
Measured acoustic propagation loss (at centre frequency), dB	6·6	6·0	6·2
Measured beam-steering loss, dB	3·38	3·85	not measurable
Calculated diffraction loss, dB	0·42	0·33	1·26
Measured delay time (2 cm transducer separation), μs	5·7	5·7	5·0
Measured delay-line centre frequency, MHz	995	985	1130
Measured delay-line 3 dB bandwidth, MHz	87·5 (8·8%)	60 (6·1%)	113 (10%)

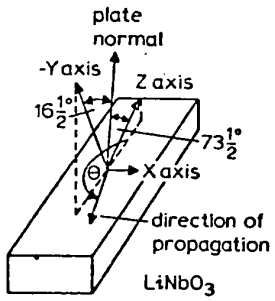

Fig. 54 Coordinate system for the crystal cuts of Table III

fraction loss (YZ cut), low beam steering loss (41½° cut) or a combination of high coupling and low diffraction (16½° cut). Fig. 54 explains the meaning of the 16½° designation in terms of the crystalline axes.

b/ Lithium tantalate (rhombohedral, point group /3m/) has similar characteristics to lithium niobate, being of similar crystal structure. While its coupling is lower, its temperature coefficients are better than those of lithium niobate.

c/ Barium sodium niobate (orthorhombic, point group /mm2/) is distinguished by its special optical characteristics. Due to its ability to withstand intense laser radiation, it performs well in non-linear optical devices such as frequency doublers and parametric oscillators.

d/ Crystalline quartz (point group /32/ or /622/) is one of the most popular crystal materials on account of its excellent mechanical properties. It can be sawed, ground and polished with relative ease. It is not water-soluble which makes processing more convenient. The disadvantage of low piezoelectric coupling is often offset by the low cost and easy availability of the crystal.

e/ Bismuth germanium oxide (cubic, point group /23/) as mentioned before, is one of the promising new materials. It has a large time-bandwidth product and some attractive fabrication properties; it can be grown at a relatively low temperature (below 1000° C) by the well-developed Czochralski technique. It is not ferroelectric and can be easily etched to form acoustic

waveguides.

f/ Lithium gallate (orthorhombic, point group /mm2/) is similar in crystal structure to barium sodium niobate. It is not ferroelectric, however, therefore does not require poling. Its coupling is higher and it is usable over a wider temperature range.

g/ Lithium iodate (hexagonal, point group /6/): a high value of piezoelectric coupling with low values of dielectric constant. It is water soluble; the crystals are grown in a water solution at about 45° C. At the same time, it is not hygroscopic, so it can be used in ordinary room atmosphere without deterioration.

h/ Cadmium sulfide (point group /6mm/), a piezoelectric semiconductor, finds limited use in bulk form because of its high acoustic attenuation. It is frequently used however, in the form of a thin polycrystalline film on top of other substrates. An example of such an application is mentioned in Section 3.1 where its photoconductive properties are utilized. The film is also employed in bulk wave transduction.

i/ Zinc oxide (point group /6mm/) has similar features and applications to cadmium sulfide, again being used mostly as a polycrystalline film overlay. Section 3.1 describes one such application, where the ZnO layer is placed over a glass substrate.

j/ PZT is a polycrystalline piezoelectric ceramic, with high coupling coefficients and low dielectric constants, but also high acoustic attenuation. Still, its large time-bandwidth

product makes it a frequently used substrate, especially at lower frequencies. The size of the individual grains in the material is about 1 μm, sufficiently large to retain ferroelectricity, yet small enough so it can be polished to small dimensions.

In addition to bulk materials, the expanding range of film-substrate combinations offers new features and sets new requirements regarding component material characteristics. The technique of heteroepitaxy (growing one single chemically different crystal material on another) offers great variety. The process of fabrication is chemical vapor deposition [12]. One example is silicon-on-sapphire with lithium niobate for surface acoustic amplification, another is the growth of ZnO film on sapphire or glass (see Section 3.1). CdS on lithium niobate is still another combination, utilizing the photoconductive characteristics of cadmium sulfide (described in Section 3.1). Combinations developed in this fashion often yield excellent properties of low attenuation, ease of handling and the facility of building surface wave devices and semiconductor devices into an integrated circuit by virtue of deposition of a piezoelectric film on the common semiconductor base.

4.2 Fabrication techniques

The problems of fabricating surface wave transducers on crystal substrates are basically similar to those of thin-film technology. Photolithographic processing, a common and well-deve-

loped technique, can be applied to surface acoustic devices, particularly at lower frequencies. When electrode spacing approaches the order of a micron, the technique proves to be less satisfactory and special processes are required. These approaches are described in this section, beginning with the standard photolithographic method.

Photolithographic processing [6]

The essence of this process is the following: the substrate is covered completely with a thin metallic film, which in turn is overlayed with photoresist. By means of a photomask, the resist is selectively exposed. The exposed resist is removed, baring the metal film underneath. The application of either chemical etching or sputter etching removes the exposed part of the film. Finally, removal of the unexposed resist reveals the desired transducer pattern in the form of a metallic film layer. (See Fig. 55). The photomasks are made from a large-scale version of the desired pattern through precise photographic reduction. A master mask is prepared first, from which copies are made by photoresist contact printing for direct use in the fabrication process. The mask is then pressed upon the device substrate which has been prepared with the metal film and photoresist overlay. The photoresist (either negative type such as Kodak KTFR or positive type such as Shipley AZ 1350) of about 1000 Å thickness is then exposed through the mask to ultraviolet light. A chemical change affecting the solubility of the resist takes place. In the following develop-

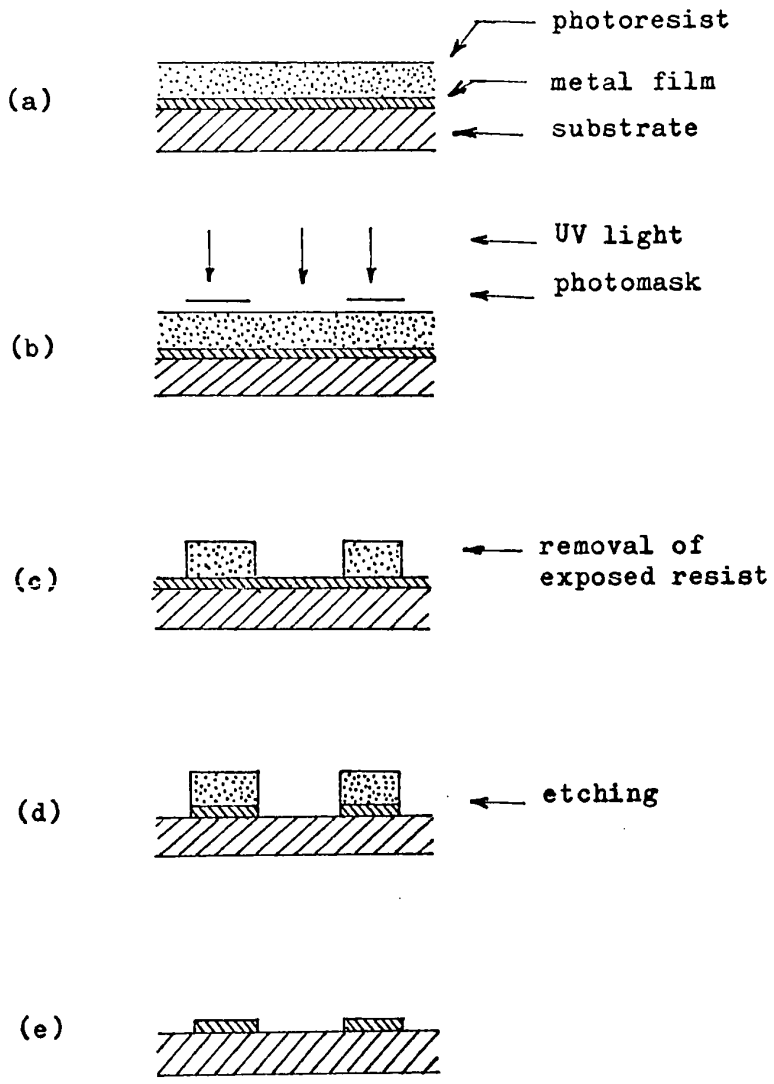

Fig. 55 Photolithographic processing

ment step, the exposed resist material is removed by the appropriate solvent, exposing the metal film underneath [37].

One way of removing the unprotected metal film is by chemical etchants, which do not attack the unexposed resist, but dissolve the metal film. This technique presents a number of problems in transducer fabrication: the etchant has a tendency to penetrate under the unexposed portions of the resist, and also tends to attack the substrate surface itself. The substrate material of course is selected for its desirable characteristics from the point of view of acoustic behaviour rather than its chemical resistance. It is also usually polished to a high degree. Chemical etching emphasizes any surface imperfection, leading to unacceptable quality, hence a low manufacturing yield for resolutions of about 5 μm or better.

An improved technique for the removal of exposed metal film is sputter etching [14]. In this process, the device samples, with the exposed resist having been removed, are placed in a vacuum container. Low pressure argon gas ($\sim 10^{-2}$ Torr) is let in which is ionized under the effect of high electric field. The samples being placed on the negative electrode, high velocity positive ions bombard the surface. While the unexposed resist absorbs these ions, the exposed metal film is gradually worn away due to metal particles being dislodged by the ions. To prevent the removal of substrate material, sputtering is terminated while some of the metal still remains. This is removed by chemical et-

ching of short duration. This etching technique eliminates the under-cutting effects of chemical etching, and permits still higher resolutions. It too, however, has certain disadvantages. Sputtered metal depositing on the inside of the glass container makes monitoring of the process difficult. Sometimes, as a result, the substrate itself is sputtered, damaging the surface finish.

A different photolithographic approach is presented by H.I. Smith at al [38]. Throughout this process, the substrate material is isolated from chemical etchants, thereby overcoming the weaknesses of the preceding techniques. It permits, therefore, the use of chemically reactive or degradable materials as substrates.

Fig. 56 illustrates the steps of the process. In this method, the photoresist is deposited directly on the substrate surface, then exposed to ultraviolet light through the optical mask. The exposed resist is removed by solvents. Metal deposition follows next, resulting in a continuous film covering substrate and unexposed resist. The manner of deposition is such that the metal particles, arriving vertically, tend to settle mostly on the horizontal surfaces, leaving a relatively thin layer on the vertical sides of the resist. When the sample is immersed in a solvent, the resist absorbs it, swelling in the process. It separates the film strips in the manner shown in Fig. 56(c), permitting the removal of the resist together with the

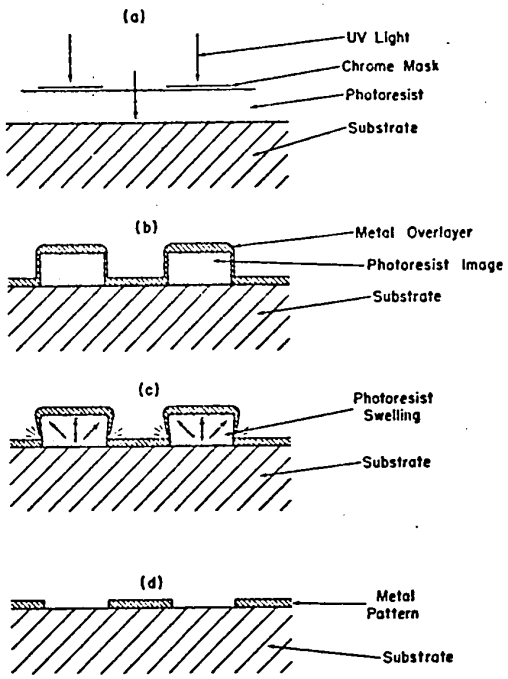

Fig.56 Improved photolithographic technique

unwanted metal film deposited on it. Fig. 56(d) shows the remaining metallic transducer pattern. Metal deposition takes place in an electron-beam evaporator, resulting in a 1000 Å to 2000 Å thickness in case of aluminum. The photoresist is the negative type, AZ 1350.

High electrode resolutions, down to the order of 1 μm are obtainable with this technique, bringing transducer fabrication technology up to the microwave range of frequencies. Because of high edge definition, the process is particularly valuable in case of substrates with naturally rough surfaces such as certain piezoelectric cramics and thin films. Light diffraction effects limit the resolutions obtainable through traditional photolithographic methods to about 0.9 μm, corresponding to about 1 GHz on YZ lithium niobate.

E.G. Lean and A.N. Broers [26] describe a technique which makes feasible the fabrication of transducers operating in the fundamental mode at frequencies as high as 2.5 GHz. It employs the precise beam of an electron microscope to expose the photoresist overlay in a fabrication sequence otherwise substantially identical to that previously described [38]. The instrument used is capable of producing an electron beam with a diameter of 25 Å, in fact smaller then required for acoustic devices operating in the S-band. (The beam is adjusted to a diameter of about 200 Å, with high beam intensity of about 10^{-9} A). While the process appears to be rather expensive for manufacturing purposes due to the high cost of

the electron-microscope, it did produce devices for experimental use, enabling researchers to explore acoustic behaviour in the microwave frequency range. The device reported by Lean and Broers for example, had transducers of 0.3 μm finger-width, separation between adjacent lines of 0.4 μm and electrode thickness of 700 Å. The substrate being YZ lithium niobate ($v = 3.45 \times 10^5$ cm/sec), the center frequency of the transducer is about 2.5 GHz.

4.3 Problems of microwave frequency operation.

There are several problems associated with efforts to operate acoustic devices at gigahertz frequencies. For one, transducer periodic spacing becomes very close, according to:

$$L = \frac{v}{f}$$

Optical photolithographic methods have a resolution limit of about 0.9 micron, corresponding to about 1 GHz on YZ lithium niobate.

Another problem is attenuation: propagation losses become significant at microwave frequencies [10], due to scattering of the surface waves by thermal phonons and surface crystalline defects, as well as to "air loading" as already mentioned in Section 2.4. Nevertheless, the effort to develop microwave acoustic techniques is a worthwhile one, because at lower frequencies one cannot obtain the wide bandwidths necessary for some applications such as radar systems. The ability to operate at the microwave frequency range opens the possibility of constructing signal pro-

cessing devices without the necessity of downconversion and consequent upconversion.

To alleviate the problem of attenuation, single crystal substrates are used, highly polished and often encapsulated to prevent surface contamination. This solution creates some additional problems of its own, having to do with the anisotropy of single crystals that requires precise alignment of the transducers with the selected crystalline direction, to avoid beam steering and associated losses. Another contributor to the total insertion loss of a microwave acoustic device is the increased transducer conversion loss. As high frequencies are approached, the dimensions of the electrode fingers are by necessity becoming smaller, therefore their resistance increases (designated as R_c in the equivalent circuits of Sections 3.3 and 3.5). In contrast to the low-frequency case where R_c was often negligible, at microwave frequencies this term becomes dominant compared to the radiation resistance R_a. This loss resistance may be reduced by the usual technique of increasing N (since the fingers are in parallel) but the consequence is reduced bandwidth. Stagger-tuning the transducers can improve the situation, i.e. building a transducer with non-uniform periodicity.

The solution to the problem of close electrode spacing has been approached with the overtone operation of transducers, i.e. operating a transducer at 1.2 GHz with periodicity designed for, say, 400 MHz. Whereas this appears to solve the fabrication

problem, efficiency of transduction is drastically reduced, resulting in high insertion loss. Overtone operation also carries the unexpected side-effect of bulk-mode generation. As illustrated in Fig. 57, a coherent bulk wave with velocity v_v will be generated by the surface wave transducer when the angle θ satisfies the relationship:

$$\cos\theta = \frac{\lambda_{volume}}{n\lambda_{surface}} = \frac{v_{volume}}{n \cdot v_{surface}}$$

where n is the order of the overtone [10]. Since v_{volume} is generally larger than $v_{surface}$ (except in particular crystalline directions where "leaky" waves propagate), at fundamental operation (n = 1) the above relation cannot be satisfied and no bulk waves originate. At harmonics of the fundamental however, it can be satisfied and volume waves will be observed. These weaknesses of overtone operation led to new fabrication techniques with the aim of extending the resolution limits of traditional photolithography and thereby enable microwave frequency operation in the fundamental mode.

The technique, described by E.G. Lean and A.N. Broers [26] accomplishes this objective up to 2-3 GHz by virtue of replacing light beam with a precise electron beam in the photo-process. The 2.5 GHz delay line reported by Lean and Broers illustrates some of the problems just mentioned: the d-c electrode resistance, R_c, of 12 aluminum finger pairs was about 18 Ω, while the radiation resistance was only about 5 Ω at resonance. The resulting mismatch

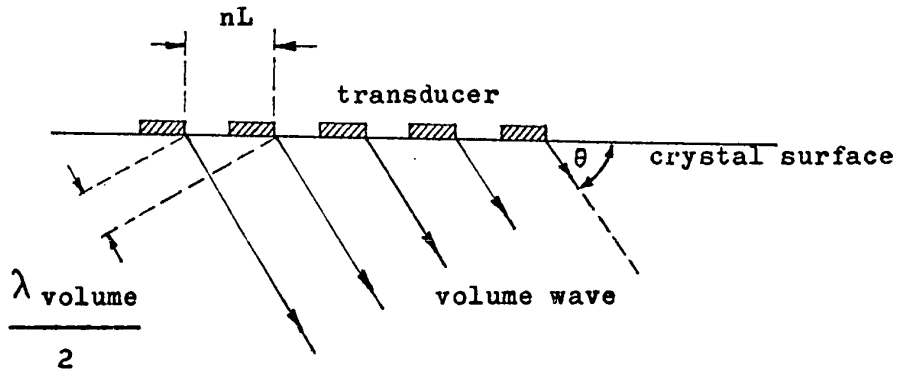

Fig. 57 Bulk wave generation in overtone operation

with respect to a 50 Ω input source resulted in a 7 db conversion loss in the transducer, in addition to the usual 3 db loss due to bi-directionality. Propagation loss for a 1.5 μsec delay line was about 9 db, amounting to a total insertion loss of 29 db.

4.4 Measurement techniques

To verify predicted performance, a set of measurements can be made on surface wave devices. To take advantage of the relatively slow propagational velocity, the favored method is the use of pulse-type input signals [50]. In this manner, the input and output signals are well separated in time and the effects of electrical feed-through (which appear practically instantaneously in the output) can be minimized. To further reduce this latter effect, metallic shielding between the ports and appropriately shielded electrical connections are used.

The measurements are of the electrical and acoustic type. The first group involves measurement of input and output signals and impedances at the electrical ports. Knowledge of input impedance is important in order to determine the necessary impedance matching circuits and to evaluate strength of coupling. Since both amplitude and phase information are required, together with frequency dependence, network analyzers or vector voltmeters are required (such as Hewlett Packard's 8410A or 8405A respectively).

The techniques used to measure acoustic parameters, i.e. velocity, amplitude or attenuation, are more specialized. Some

unique methods have been developed, some based on probing the piezoelectric field by means of metallic contact, some on optical probing.

An example of the first approach is one reported by B.A. Richardson and G.S. Kino [30]. The key element in their measuring apparatus is a movable fine tungsten point probe, illustrated in Fig. 58(a). The probe, placed in contact with the surface of the piezoelectric medium, detects the electrical potential associated with the propagating surface wave. The tungsten wire has a 0.015" diameter; it is further sharpened by electrochemical etching to a fine point. When pressed against the surface, a contact area of less than 25 μm in diameter results. The electric field being proportional to the acoustic displacement, the measurement provides information about surface wave amplitude and phase. By moving the probe along the surface in the direction of propagation, surface attenuation may be measured. Also, by moving the probe in a direction parallel to the wavefront, the fine structure of the power distribution within the acoustic beam can be observed, and the effects of diffraction and beam-steering evaluated. Fig. 58(b) shows the block diagram of the measuring equipment. One disadvantage of this method is that it is applicable to piezoelectric substrates only. The size of the contact area of the probe also limits the highest measurable frequency of this scheme.

The optical techniques do not have these limitations. Employing the narrow, focused beam of a laser to probe the surface,

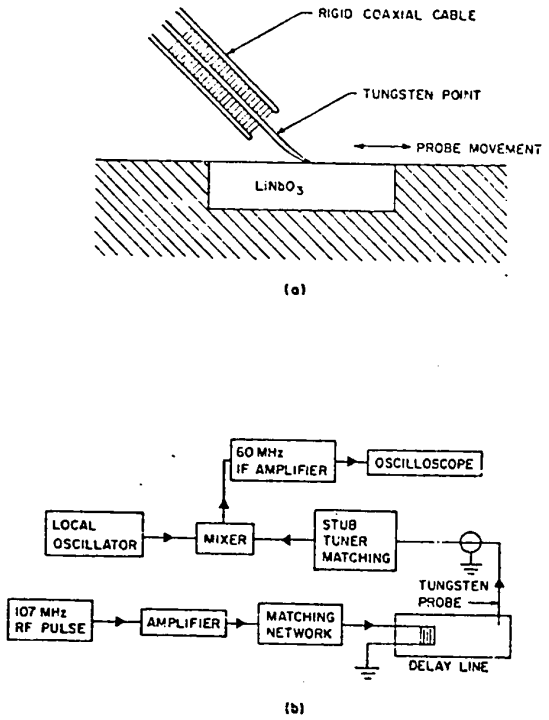

Fig. 58 Surface wave measurement by flexible probe

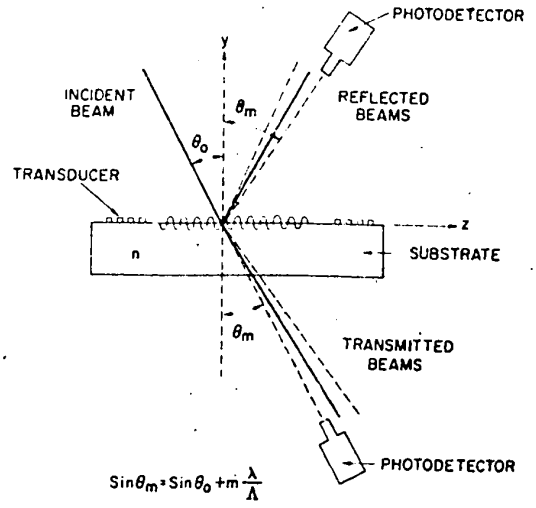

Fig. 59 Light beam diffraction by surface waves

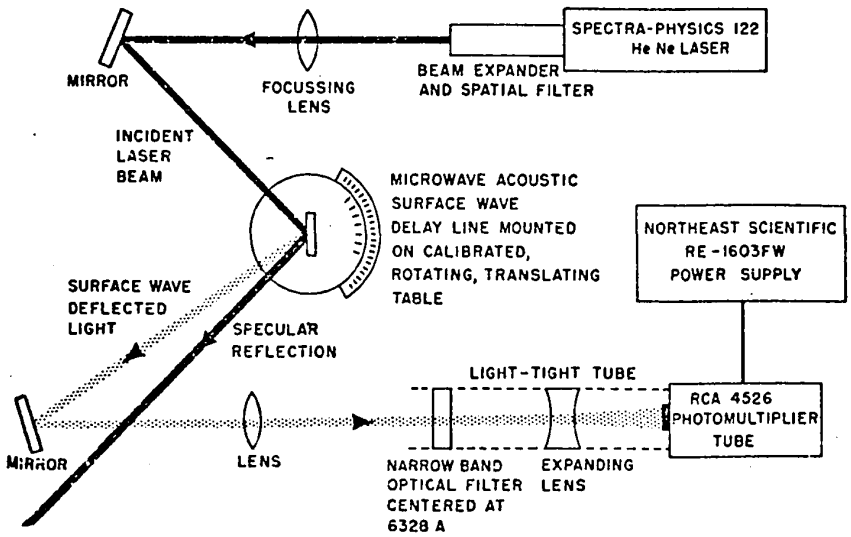

Fig. 60 Measurement of surface waves by light diffraction

they achieve resolutions suitable for microwave frequencies. At the same time, piezoelectricity is not a requirement. The principles of measurement by light diffraction have been known for some time and recently applied to acoustic devices. Lean and Powell [25] presented an analysis of these techniques and the results of their use in studying attenuation, harmonic generation and transducer performance on YZ lithium niobate. The detailed work of J. Krokstad analyzes the properties of quartz by similar methods [23].

Fig. 59 illustrates the basic arrangement of the optical experiment. The surface corrugations represent the propagating Rayleigh waves. The incident laser beam encounters a periodically shifting surface and thus will diffract on reflection into many side orders. Some of the incident light will penetrate the substrate and pass through it. This transmitted beam can be detected as well, since it also suffers diffraction, hence carrying information about the surface wave. In this case, diffraction is due to two factors: surface deformation, resulting in variation of the amount of crystal material the beam must pass through, and a periodic variation in the index of refraction as the material contracts and expands due to the passage of pressure waves. The fractions of reflected and transmitted beams depend on surface quality and transparency of the crystal. Either of the two may be used for measurement, resulting in a variety of arrangements. One of them, used by Slobodnik and Budreau [35] in measuring the properties of $Bi_{12}GeO_{20}$, is shown in Fig. 60. It employs reflected

light for the probing of the surface. A phase-grating type of diffraction results from surface deformation with the diffraction angles being related to the incident angle as follows:

$$\sin\theta_m = \sin\theta_o + m\frac{\lambda}{\Lambda} \qquad m = 0, \pm 1, \pm 2, \ldots$$

where θ_m is the diffraction angle of the m-th order with respect to the surface normal, θ_o is the angle of incidence, λ and Λ are the optical and acoustic wavelengths.

Surface wave velocity measurements may be made by detecting for example the first order diffracted beam and calculating Λ from the above relationship (assuming optical and acoustic frequencies are known). Another expression states the ratio of intensities between the various diffracted beams and the specularly reflected beam [25]:

$$\frac{I_m}{I_o} = J_m^2(\nu) \qquad m = 1,2,3, \ldots$$

where $J_m(\nu)$ is the m-th order Bessel function. Its argument, ν is a function of surface wave amplitude, δ_o:

$$\nu = \frac{4\pi}{\lambda}\delta_o \cdot \cos\theta_o$$

the surface wave deformation being expressed as:

$$\delta = \delta_o \cos(\omega_s t - k_s x_3)$$

where x_3 is the direction of propagation, k_s is the acoustic wavenumber and ω_s is the acoustic angular frequency.

These relationships make possible the measurement of surface wave intensities and attenuation, the latter by comparing intensities at different points along the propagation path. The arrangement of Fig. 60 facilitates this by permitting lateral movement of the sample device.

A variety of tests have been performed, analyzing the various surface wave loss mechanisms and determining the relationships between attenuation and frequency, linearity and input power, harmonic generation and frequency, etc. [25]. Diffraction and beam steering experiments can be performed even at microwave frequencies. Utilizing the narrow laser beam, the acoustic beam profile is probed at various points along the propagation path. The degree of distortion in the beam cross section indicates the accuracy of alignment between the transducer axis and the desired crystalline direction.

Scattering characteristics of transducers may be tested by placing the laser beam in front of the transducer and observing the intensities of light diffracted by incident and reflected acoustic signals. The signals are again in the form of pulses for time-separation of the two signals to be measured. Varying the electrical load on the transducer allows observation of its behaviour as a function of terminating conditions.

SUMMARY

Elastic stress-waves, propagating on crystal surfaces, promise the development of a new family of devices. They can perform circuit functions heretofore provided by conventional devices of far greater physical dimensions. A mathematical analysis of these waves identifies them as being a combination of longitudinal and transverse displacements. The exact nature of the displacement and its variation with depth below the surface depends on the particular boundary conditions existing in the vicinity of the surface. The resulting waves are known as Rayleigh, Rayleigh-type, Stoneley, Love, and electroacoustic waves. All of them share the important property of a low velocity of propagation, hence small wavelengths compared to those of electromagnetic waves. It is this property which opens up the possibility of fabricating high frequency devices on a miniature scale. The variety of circuit functions is due to the accessibility of these waves on the crystal surface, their ability to be guided, focused, amplified and tapped.

An important aspect of surface wave operation is the launching and reception of the elastic waves. Conversion of electrical signals to stress waves on the crystal and back to electric signals is the function of transducers. This task is greatly simplified by the use of piezoelectric crystals. In these materials, the appearance of an electric field over the input area generates

elastic contractions and expansions of the crystal surface. These movements, associated with a traveling electric field, propagate over the surface to the output area where the arriving electric field is sensed and detected. The transducers performing the function of conversion are usually metal electrodes deposited on the crystal surface by photolithographic methods. The most frequently used type has the shape of two comb-like structures facing each other, teeth interleaved in an interdigital fashion. The spacing of the teeth, or digits, corresponds to the acoustic wavelength on the crystal surface, usually 5 orders of magnitude smaller than electromagnetic wavelengths.

The behaviour of these transducers can be analyzed with the help of equivalent electric circuits. The analysis indicates a strong resemblance to the characteristics of antenna arrays, including their frequency dependence and the concept of radiation immittance. The results yield expressions relating circuit behaviour to physical characteristics of the transducer.

Design techniques, based on the results of the analysis, have been developed, by which certain desired characteristics can be achieved through the manipulation of such physical parameters as electrode spacing and length, as well as the number of electrode pairs. The practical results of tnese techniques make available such devices as broadband delay lines, dispersive filters, matched filters for radar applications and the like.

Another contributor to overall device characteristics, besides transducers, is of course the crystal substrate itself. The ultimate success of surface wave devices hinges on the ability to locate suitable materials which combine to the best possible degree a number of important characteristics. These include: strong piezoelectricity, low loss, good temperature stability, ability to withstand the rigors of fabrication, easy availability and not the least, low price. A number of promising materials have been identified and the search continues for better ones.

One of the attractive aspects of acoustic surface wave devices is the fortunate fact, that most manufacturing techniques required for their production have already been well developed. The use of integrated circuit technology should contribute to the availability of cost-competitive devices. Many problems are still to be overcome, particularly those related to microwave frequency operation. This field definitely has a place for micro-sized circuit elements, yet the small wavelengths of elastic waves, normally an attractive feature, become the source of fabrication difficulties. As the spacing between electrodes equals the surface wavelengths, separations of less than a micron are required for frequencies above 1 GHz.

Part of the present activity in the electroacoustic field is aimed at developing the necessary techniques to fabricate UHF transducers and amplifiers, the latter to overcome the increased

attenuation at microwave frequencies. Layered substrate materials are also being investigated. Their ability to combine desired properties of different materials will be put to use at these high frequencies when expected developments in heteroepitaxy technology are realized. At lower frequencies, the construction of delay lines is the object of active research. Achieving delays in the order of 16 ms would bring about the possibility of storing a complete TV frame for comparison with previous ones. The difference between adjacent frames being usually small, this small change only could be transmitted, resulting in bandwidth reduction of a factor of about 10. Devices arising from the interaction between surface acoustic waves and light are also the subject of investigation. Developments in this area may result in new types of display devices and methods of light modulation.

The field of surface waves is a new and developing area. While many of the concepts are still in the experimental stage, practical devices are beginning to be used in radar and communication systems; early realizations of a promising future for the family of surface acoustic devices.

REFERENCES

1. L. Altman,"Tapping Microwave Acoustics", Electronics, Vol.42, No. 23, pp. 94-96, November 10, 1969

2. E.A. Ash, R.M. De LaRue, and R.F. Humphryes,"Microsound Surface Waveguides", IEEE Trans. Microwave Theory Tech., Vol. MTT-17, No. 11, pp. 882-892, November 1969.

3. B.A. Auld and G.S. Kino,"Normal Mode Theory for Acoustic Waves and its Application to the Interdigital Transducer", IEEE Trans. Electron Devices, Vol. ED-18, No. 10, pp. 909-920, October 1971.

4. B.A. Auld, D.A. Wilson, D.K. Winslow and E. Young,"Control of Acoustic Surface Waves with Photoconductive CdS Film", Appl. Phys. Lett., Vol. 18, No. 8, pp. 339-341, April 15, 1971.

5. A.J. Bahr, R.E. Lee and A.F. Podell,"The Grating Array: a New Surface Acoustic Wave Transducer", Proc. IEEE, Vol. 60, No. 4, pp. 443-444, April 1972.

6. R.W. Berry, P.M. Hall and M.T. Harris,"Thin Film Technology", Van Nostrand, 1965

7. H.L. Bertoni,"Piezoelectric Rayleigh Wave Excitation by Bulk Wave Scattering", IEEE Trans. Microwave Theory Tech., Vol. MTT-17, No. 11, pp. 873-882, November 1969.

8. M. Bruun, S. Ludvik and C.F. Quate,"Field Effect Transistors on Epitaxial GaAs as Transducers for Acoustic Surface Waves", App. Phys. Lett., Vol. 18, No. 4, pp. 118-120, February 15, 1971.

9. J.J. Campbell and W.R. Jones,"A Method for Estimating Optimal Crystal Cuts and Propagation Directions for Excitation of Piezoelectric Surface Waves", IEEE Trans. Sonics Ultrason., Vol. SU-15, No.10, pp. 209-217, October 1968

10. H. Carr,"The Generation and Propagation of Acoustic Surface Waves at Microwave Frequencies", IEEE Trans. Microwave Theory Tech., Vol. MTT-17, No. 11, pp. 845-855, November 1969.

11. L.A. Coldren and G.S. Kino,"Monolithic Acoustic Surface Wave Amplifier", Appl. Phys. Lett., Vol. 18, No. 8, pp. 317-319 April 15, 1971.

12. J.H. Collins and P.J. Hagon,"Amplifying Surface Acoustic Waves", Electronics, Vol. 42, No. 25, pp. 102-111, December 8, 1969.

13. J.H. Collins and P.J. Hagon,"Applying Surface Wave Acoustics", Electronics, Vol. 42, No. 23, pp. 97-103, November 10, 1969.

14. P.D. Davidse,"RF Sputter Etching--a Universal Etch", J. Electrochem. Soc., Vol. 116, pp. 100-103, January 1969

15. H. Engan,"Excitation of Elastic Surface Waves by Spatial Harmonics of Interdigital Transducers", IEEE Trans. Electron Devices, Vol. ED-16, No. 12, December 1969.

16. G.W. Farnell,"Properties of Elastic Surface Waves", in Physical Acoustics, Vol. 6, W.P. Mason and R.N. Thurston, Eds. New York: Academic Press, 1970.

17. H.M. Gerard, G.W. Judd and M.E. Pedinoff,"Phase Corrections for Weighted Acoustic Surface Wave Dispersive Filters", IEEE Trans. Microwave Theory Tech. (Correspondance), Vol. MTT-20, No. 2, pp. 188-192, February 1972.

18. C.S. Hartmann, W.S. Jones and H. Vollers,"Wideband Unidirectional Interdigital Surface Wave Transducers", IEEE Trans. Sonics Ultrason., Vol. SU-19, No. 7, pp. 378-381, July 1972.

19. W.S. Jones, C.S. Hartmann and T.D. Sturdivant, "Second Order Effects in Surface Wave Devices", IEEE Trans. Sonics Ultrason., Vol. SU-19, No. 7, pp. 368-377, July 1972.

20. W.S. Jones, C.S. Hartmann and L.T. Claiborne, "Evaluation of Digitally Coded Acoustic Surface Wave Matched Filters", IEEE Trans. Sonics Ultrason., Vol. SU-18, No. 1, January 1972.

21. G.S. Kino and T.M. Reeder, "A Normal Mode Theory for the Rayleigh Wave Amplifier", IEEE Trans. Electron Devices, Vol. ED-18, No. 10, October 1971.

22. G.S. Kino and H. Matthews, "Signal Processing in Acoustic Surface Wave Devices", IEEE Spectrum, Vol. 8, No. 8, August 1971.

23. J. Krokstad, "Scattering of Light by Ultrasonic Surface Waves in Crystals", Electronics Research Lab., Norwegian Institute of Technology, Trondheim, Norway, Rept. TE-93, October 1967.

24. K.M. Lakin and D. Pennuri, "Surface Waves in Layered Media on Sapphire Substrates", paper presented at the 1971 IEEE Ultrasonics Symp., December 6-8, 1971, Miami Beach, Fla., U.S.A.

25. E.G.H. Lean and C.G. Powell, "Optical Probing of Surface Acoustic Waves", Proc. IEEE, Vol. 58, No. 12, December 1970.

26. E.G.H. Lean and A.N. Broers, "Microwave Surface Acoustic Delay Lines", Microwave J., Vol. 13, No. 3, pp. 97-101, March 1970.

27. R.E. Lee and R.M. White, "Elastic Wave Generation by a Gunn Effect Oscillator Coupled to a Piezoelectric", Appl. Phys. Lett., Vol. 16, No. 9, pp. 343-346, May 1, 1970.

28. F.G. Marshall, E.G.S. Paige and A.S. Young, "New Unidirectional Transducer and Broadband Reflector of Acoustic Surface Waves", Electron. Lett., Vol. 7, No. 20, pp. 638-640, October 21, 1971.

29. A.H. Meitzler, "Piezoelectric Transducer Materials and Techniques for Ultrasonic Devices Operating Above 100 MHz", in Ultrasonic Transducer Materials, O.E. Mattiat Ed. New York: Plenum Press, 1971.

30. C.F. Quate and G. Cambon, "Dispersive Rayleigh Waves on Quartz", Electron. Lett., Vol. 5, No. 16, pp. 402-403, August 21, 1969.

31. B.A. Richardson and G.S. Kino, "Probing of Elastic Surface Waves in Piezoelectric Media", Appl. Phys. Lett., Vol. 16, No. 2, pp. 82-84, January 15, 1970.

32. H. Sabine and P.H. Cole, "Acoustic Surface Wave Devices--a Survey", Proc. IREE Australia, Vol. 32, No. 12, pp. 445-458, December 1971.

33. C.P. Sandbank and M.B.N. Butler, "Acoustic Surface Waves on Isopaustic Glass", Electron. Lett., Vol. 7, No. 16, pp. 499-501, August 26, 1971.

34. M.B. Schulz and M.G. Holland, "Temperature Dependence of Surface Acoustic Wave Velocity in Lithium Tantalate", IEEE Trans. Sonics Ultrason., Vol. SU-19, No. 7, pp. 381-384, July 1972.

35. A.J. Slobodnik and A.J. Budreau, "Acoustic Surface Wave Loss Mechanisms on $Bi_{12}GeO_{20}$ at Microwave Frequencies", J. Appl. Phys., Vol. 43, No. 8, pp. 3278-3283, August 1972.

36. A.J. Slobodnik and T.L. Szabo, "New High-coupling Low-diffraction Cut for Acoustic Surface Waves on $LiNbO_3$", Electron. Lett., Vol. 7, No. 10, pp. 257-258, May 20, 1971.

37. H.I. Smith, "Method for Fabricating HF Surface Wave Transducers", Review of Sci. Instr., Vol. 40, pp. 729-730, May 1969.

38. H.I. Smith, F.J. Bachner and N. Efremov, "A High-yield Photolithographic Technique for Surface Wave Devices", J. Electrochemical Soc., Vol. 118, pp. 821-825, May 1971.

39. W.R. Smith, H.M. Gerard, J.H. Collins, T.M. Reader and H.J. Shaw, "Analysis of Interdigital Surface Wave Transducers by Use of an Equivalent Circuit Model", IEEE Trans. Microwave Theory Tech., Vol. MTT-17, No. 11, pp. 856-864, November 1969.

40. W.R. Smith, H.M. Gerard, J.H. Collins, T.M. Reader and H.J. Shaw, "Design of Surface Delay Lines with Interdigital Transducers", IEEE Trans. Microwave Theory Tech., Vol. MTT-17, No. 11, pp. 865-873, November 1969.

41. W.R. Smith, H.M. Gerard and W.R. Jones, "Analysis and Design of Dispersive Interdigital Surface Wave Transducers", IEEE Trans. Microwave Theory Tech., Vol. MTT-20, No. 7, pp. 458-471, July 1972.

42. W.R. Smith and H.M. Gerard, "Differences Between In-line and Cross-field Three-port Circuit Models for Interdigital Transducers", IEEE Trans. Microwave Theory Tech., Vol. MTT-19, No. 4, pp. 416-417, April 1971.

43. E. Stern, "Microsound Components, Circuits and Applications", IEEE Trans. Microwave Theory Tech., Vol. MTT-17, No. 11, pp. 835-844, November 1969.

44. R.H. Tancrell and M.G. Holland, "Acoustic Surface Wave Filters", Proc. IEEE, Vol. 59, No. 3, pp. 393-404, March 1971.

45. F.W. Voltmer, R.M. White and C.W. Turner, "Magnetostrictive Generation of Surface Waves", Appl. Phys. Lett., Vol. 15, No. 5, pp. 153-154, September 1, 1969.

46. F.W. Voltmer, E.P. Ippen, R.M. White, T.C. Lim and G.W. Farnell, "Measured and Calculated Surface Wave Velocities", Proc. IEEE, Vol. 56, No. 9, pp. 1634-1635, September 1968.

47. F.S. Welsh, "Surface Wave Temperature Coefficients on Lithium Tantalate", IEEE Trans. Sonics Ultrason., Vol. SU-18, No. 4, pp. 108-109, April 1971.

48. R.M. White, "Surface Elastic Wave Propagation and Amplification", IEEE Trans. Electron Devices, Vol. ED-14, No. 4, pp. 181-189, April 1967.

49. R.M. White, "Stabilizing Surface Wave Devices", Electron. Lett., Vol. 8, No. 6, pp. 142-143, March 23, 1972.

50. R.M. White, "Surface Elastic Waves", Proc. IEEE, Vol. 58, No. 8, pp. 1238-1276, August 1970.